Distinct evolutionary trajectories of neuronal and hair cell nicotinic acetylcholine receptors

Irina Marcovich[1], Marcelo J. Moglie[1], Agustín E. Carpaneto Freixas[1], Anabella P. Trigila[1], Lucia F. Franchini[1], Paola V. Plazas[2], Marcela Lipovsek*[1,3] and Ana Belén Elgoyhen*[1,2]

[1] Instituto de Investigaciones en Ingeniería Genética y Biología Molecular "Dr. Héctor N. Torres" (INGEBI), Consejo Nacional de Investigaciones Científicas y Técnicas (CONICET), Buenos Aires, Argentina.

[2] Instituto de Farmacología, Facultad de Medicina, Universidad de Buenos Aires, Buenos Aires, Argentina.

[3] Centre for Developmental Neurobiology, King's College London, Institute of Psychiatry, Psychology and Neuroscience, Guy's Campus, London SE1 1UL.

* These authors contributed equally.

Correspondence should be addressed to Marcela Lipovsek (marcela.lipovsek@kcl.ac.uk)

ABSTRACT

The expansion and pruning of ion channel families has played a crucial role in the evolution of nervous systems. Remarkably, with a highly conserved vertebrate complement, nicotinic acetylcholine receptors (nAChRs) are unique among ligand-gated ion channels in that members of the family have distinct roles in synaptic transmission in non-overlapping domains, either in the nervous system, the inner ear hair cells or the neuromuscular junction. Here, we performed a comprehensive analysis of vertebrate nAChRs sequences, single cell expression patterns and comparative functional properties of receptors from three representative tetrapod species. We show that hair cell nAChRs underwent a distinct evolutionary trajectory to that of neuronal receptors. These were most likely shaped by different co-expression patterns and co-assembly rules of component subunits. Thus, neuronal nAChRs showed high degree of coding sequence conservation, coupled to greater co-expression variance and conservation of functional properties across tetrapod clades. In contrast, hair cell α9α10 nAChRs exhibited greater sequence divergence, narrow co-expression pattern and great variability of functional properties across species. These results point to differential substrates for random change within the family of gene paralogs that relate to the segregated roles of nAChRs in synaptic transmission.

Significance statement

Our work exploits several peculiarities of the family of vertebrate nicotinic acetylcholine receptors (nAChRs) to explore the evolutionary trajectories of a ligand-gated ion channel family. By performing a comprehensive comparative analysis of nAChR subunits coding sequences, single cell expression patterns and functional properties we found a contrasting evolutionary history between nAChRs with widespread expression in the nervous system compared to those with isolated expression in the inner ear. Evolutionary changes were focused on differences in co-expression and co-assembly patterns for the former and coding sequences in the latter. This multidisciplinary approach provides further insight into the evolutionary processes that shaped the nervous and sensory systems of extant animals.

INTRODUCTION

The superfamily of pentameric ligand-gated ion channels (LGIC) has an extended evolutionary history and is present in all three life domains (1-3). Extant members of the superfamily include eukaryote Cys-loop receptors that respond to acetylcholine (ACh), γ-aminobutyric acid (GABA), glycine or serotonin, invertebrate LGICs that respond to GABA, glutamate, ACh, serotonin and histamine, as well as prokaryote pH and GABA sensitive receptors, among others (1, 3-8). Nicotinic acetylcholine receptors (nAChRs) are a major branch of the Cys-loop LGIC superfamily (7, 9). To date, 17 different nAChR subunits have been described in the main vertebrate clades: α1-α10, β1-β4, δ, ε and γ (7, 8). These paralogous genes are proposed to derive from 5 paralogons, with the entire complement of extant subunits present in the vertebrate ancestor (10). Vertebrate nAChRs are non-selective cation channels that participate in numerous processes, most prominently neuromuscular junction (11, 12), inner ear efferent (13) and neuronal (14, 15) synaptic transmission.

Functional nAChRs are homomeric, comprising five identical subunits, or heteromeric, formed by at least two different subunits (7, 15, 16). The rules that govern the combinatorial assembly of functional nAChRs are complex and for the most part unknown. Some nAChR subunits can combine with other numerous, albeit specific, subunits. In contrast, some subunits can only form functional receptors with a limited subset (7, 16). This segregation has given rise to subgroups of vertebrate nAChRs named for their initially described tissue of origin and main functional location. Thus, neuronal nAChRs are formed by multiple combinations of α2-α7 (and α8 in non-mammals) and β2-β4 subunits, comprising a wide combinatorial range with alternative stoichiometries (15-17). Muscle receptors show tighter co-assembly rules. They have a typical $\alpha1_2\beta1\gamma\delta$ (or $\alpha1_2\beta1\varepsilon\delta$) stoichiometry and do not co-assemble with non-muscle subunits (16, 18). Finally, the hair cell nAChR has a very strict co-assembly constraint, being formed exclusively by α9 and α10 subunits (19-21). While α9 subunits can form functional homomeric receptors (22, 23), these are unlikely to play a major role in inner ear hair cells in vivo (24). Although the α9 and α10 subunits were initially classified as a neuronal, the α9α10 receptor does not appear to be functionally present in the brain (25). A consequence of the differences in co-assembly rules between the three subgroups of nAChRs is that, while muscle cells can toggle between at least two receptor variants and neurons are capable of expressing a great diversity of nAChRs, hair cells express only one type.

The complement of nAChR subunits is highly conserved across vertebrates and even more so in tetrapods (1, 10). This suggests a high gene family-wide negative selection pressure for the loss of paralogs and highlights the functional relevance of each individual subunit across the vertebrate clade. However, given the major differences in co-expression patterns and co-assembly rules that

79 distinguish the subgroups of nAChRs, in particular the contrast between neuronal and hair cell
80 receptors, distinct evolutionary trajectories most likely took place in different members of the
81 family. On the one hand, if only one (functionally isolated) receptor is expressed by a given cell type,
82 then selection pressure could have acted on stochastic changes of the coding sequence of
83 component subunits that altered receptor function. Such changes would not have resulted in
84 deleterious effects on other nAChRs given the restricted expression pattern of the subunits. The
85 aforesaid process could have dominated the evolutionary history of the hair cell α9α10 receptor. On
86 the other hand, widely expressed subunits that co-assemble into functional receptors with multiple
87 others have been most probably subjected to strong negative selection pressure. Changes in the
88 coding sequence that lead to changes in functional properties may have had deleterious effects on
89 alternative receptor combinations expressed in different cell types. In this case, functional
90 diversification could have arisen from stochastic changes in the expression patterns of receptor
91 subunits, resulting in a given cell changing the subtype of receptor it expresses, while preserving
92 individual subunit functionality. Such processes could have dominated the evolutionary history of
93 neuronal nAChRs. These contrasting theoretical scenarios bring forward three predictions for the
94 evolutionary history of nAChRs across the vertebrate clade. First, isolated (hair cell) subunits may
95 show coding sequence divergence while widespread (neuronal) subunits a high degree of coding
96 sequence conservation. Second, isolated subunits may show low co-expression variation while
97 widespread subunits a great variability in co-expression patterns. Finally, isolated receptors may
98 present divergent functional properties across species resulting from changes in coding sequences,
99 while widespread receptors may show highly conserved functional properties when formed by the
100 same subunits.

101 To test these predictions, we studied the molecular evolution and the variability in expression
102 pattern, coupled to co-assembly potential, of vertebrate nAChR subunits. Furthermore, we
103 performed a comprehensive comparative analysis of the functional properties of the hair cell
104 (α9α10) and the two main neuronal (α7 and α4β2) nAChRs from three representative species of
105 tetrapods. In close agreement with the aforementioned predictions, neuronal subunits showed high
106 degree of sequence conservation and great variability in co-expression patterns. Additionally, the
107 functional properties of both α7 and α4β2 receptors did not differ across tetrapods. In contrast, the
108 isolated hair cell α9α10 nAChRs showed the highest degree of sequence divergence and no co-
109 expression variability. Moreover, the functional properties of α9α10 receptors from representative
110 species of tetrapods showed unprecedented divergence, potentially echoing the evolutionary history
111 of vertebrate auditory systems. In summary, here we present strong evidence supporting the notion
112 that, within the family of paralog genes coding for nAChR subunits, receptors belonging to different

113 subgroups (hair cell or neuronal) underwent different evolutionary trajectories along the tetrapod
114 lineage that were potentially shaped by their different co-expression patterns and co-assembly rules.
115 Furthermore, we propose that it is the difference in the most probable substrate for random change
116 and subsequent selection pressure that separate the contrasting evolutionary histories of nAChRs
117 subgroups.

118

RESULTS

Amino acid sequence divergence and co-expression patterns differentiate neuronal from hair cell nAChR subunits

The comparative analysis of gene paralogs provides the opportunity to test predictions about the evolutionary history of a gene family. To study the degree of conservation of coding sequences in subgroups of nAChRs we performed an exhaustive evaluation of sequence divergence of vertebrate nAChR subunits. The analysis included amino acid sequences from 11 species of birds, reptiles and amphibians, all groups that were notably under-represented in previous work (1, 26-30) and are of particular importance to help resolve differences between clades. Overall, we analysed 392 sequences from 17 nAChR subunits belonging to 29 vertebrate species (Table S1). Based on sequence identity, the family of nAChR subunits can be split into four groups: α, non-α, α7-like and α9-like (Fig. 1 and S1-S2). As previously reported with smaller datasets (26, 28), the present extended analysis showed that α10 subunits are unique in presenting a segregated grouping of orthologues with non-mammalian α10 subunits as a sister group to all α9 subunits, and mammalian α10 subunits an outgroup to the α9/non-mammalian α10 branch (Fig. 1). This may relate to the overall low %seqID of all vertebrate α10 subunits, coupled to high sequence conservation within individual clades (Table S2). Interestingly, a close inspection of the cumulative distribution of within and between-clade %seqID suggests that both α9 and α10 hair cell subunits may have accumulated a high proportion of their overall aminoacid changes at the mammalian/sauropsid split, while sequence divergence in neuronal subunits appears distributed throughout the phylogeny (Fig S3). To further test this, we searched for site-specific evolutionary shifts in aminoacid biochemical state between clades ((31) and SI methods) and found that both α9 and α10 subunits have a high number of sites showing potential functionally significant aminoacid changes when comparing the mammalian vs sauropsid clades (Fig. 1B – red bars and Table S3). In contrast, neuronal subunits fail to show between-clade functional divergence at the sequence level (Fig. 1B and Table S3). Overall, the extended molecular evolution analysis of nAChR subunits showed that while neuronal subunits were highly conserved across all vertebrate clades, α9 and α10 hair cell subunits showed a greater degree of between-clade sequence divergence that differentiates mammalian and sauropsid subunits.

The capability to co-assemble into functional receptors and the co-expression of nAChR subunits within a given cell delineate the complement of receptors that shape its nicotinic ACh response. Numerous heterologous expression experiments and subunit-specific pharmacological studies have outlined a comprehensive repertoire of functionally validated pentameric assemblies (Table S6 and

152 references therein). However, no systematic gene expression analysis that explores the potential
153 spectrum of nAChRs in a given cell type has been performed. In order to evaluate co-expression
154 patterns, we performed a meta-analysis of gene expression data from 10 recent single-cell
155 transcriptomic studies (Table S4). First, from the gene expression matrices we identified the
156 repertoire of nAChR subunits detected in each single cell (Fig. S4). Subsequently, we used a Bayesian
157 approach (32) to estimate the likelihood of a gene being expressed at any given average level in a
158 given cell type (Table S5, Fig. 2 and Fig. S5). We next combined this data with the catalogue of
159 validated nAChR pentamers (Table S6) and outlined the potential complement of pentameric
160 receptors present in each cell type, by identifying the subunit combinations that are present within a
161 10-fold, 100-fold or 1000-fold range of expression level or altogether absent (Fig. S6A). As expected,
162 neurons express a range of neuronal nAChR variants with major neuronal types identified by their
163 well characterised nAChRs. For example, visceral motor neurons from thoracic sympathetic ganglia
164 express receptors containing α3 and β4 subunits, while cortical neurons express receptors
165 containing α4, β2 and α7 subunits. Ventral midbrain dopaminergic neurons express high levels of the
166 α6 subunit, together with β2 and β3 subunits and variable levels of α3, α4 and α5 subunits.
167 Receptors containing the α2 subunit are observed in different types of retinal neurons (Fig. 2). Also,
168 GABAergic, glutamatergic and dopaminergic neurons from hypothalamus, ventral midbrain and/or
169 sympathetic ganglia present noticeably different potential complements of nAChRs (Fig. S6A).
170 Differences in potential nAChRs composition can be observed even between closely related cell
171 types. For example, two subtypes of cortical pyramidal neurons that differ on their projection targets
172 (33) show a significant difference in the expression level of the α5 subunit (Fig. S6B), indicating they
173 could differ on the ratio of α4β2/α4α5β2 receptors on the plasma membrane. Finally, inner ear hair
174 cells co-express high levels of α9 and α10 subunits (Fig. 2 and S6C).

175 Taken together the analysis of aminoacid sequences and co-expression patterns indicates that,
176 whereas the α9 and α10 subunits have a restricted expression pattern, they also have the highest
177 clade-specific sequence divergence. On the contrary, neuronal nAChRs present higher sequence
178 conservation together with a widespread expression pattern.

179 **Divergence of biophysical properties differentiates neuronal from hair cell nAChRs**

180 The restricted co-expression pattern of hair cell α9 and α10 nAChR subunits (Fig. 2) and their
181 exclusive co-assembly with each other (19-21), together with their higher level of between-clade
182 sequence divergence (Fig. 1 and S3), indicate the potential for functional innovations across clades
183 through coding sequence changes. In contrast, the high conservation of neuronal subunits (Fig. 1 and
184 Table S3) may have resulted in highly conserved functional properties of neuronal receptors

assembled from the same subunits. We experimentally tested this prediction by performing a comprehensive side-by-side comparison of the functional properties of the two main neuronal, α4β2 and α7 nAChRs, and the hair cell α9α10 nAChR from three representative species of tetrapod clades. To this end, we injected *Xenopus laevis* oocytes with the corresponding cRNAs and characterised the biophysical properties of ACh responses.

Oocytes injected with rat (*Rattus norvegicus*), chicken (*Gallus gallus*) or frog (*Xenopus tropicalis*) α4 and β2 cRNAs responded to ACh and showed the characteristic two-component ACh dose-response curves that correspond to the well described $(\alpha4)_3(\beta2)_2$ and $(\alpha4)_2(\beta2)_3$ prevalent stoichiometries (Fig. 3A, Table S8 and (34)). Oocytes injected with rat, chicken or frog α7 cRNA responded to ACh with similar apparent affinities (Fig. 3A, Table S8). Finally, rat, chicken and frog α9 and α10 subunits formed functional heteromeric α9α10 nAChRs that responded to ACh in a concentration-dependent manner (Fig. 3A and (19, 28)). The frog α9α10 receptor exhibited a significantly higher apparent affinity than its amniote counterparts ($p = 0.0026$ (vs rat), $p = 0.0060$ (vs chick) – Fig. 3A and Table S8).

While the α4 and β2 subunits participate exclusively in heteropentameric receptor assemblies, rat α9 (Fig. 3B and (22)), chicken α9 (Fig. 3B and (23))and frog α9 (Fig. 3B) subunits assembled into functional homomeric receptors. In contrast, rat α10 subunits cannot form functional receptors on their own (Fig. 3B and (19)). Surprisingly, both chicken α10 (Fig. 3B and (23)) and frog α10 (Fig. 3B) subunits assembled into functional homomeric receptors.

A defining feature of nAChRs is their desensitisation upon prolonged exposure to the agonist (35). Rat and chicken neuronal α4β2 receptors are characterised by slow desensitisation kinetics (28, 36). As shown in Fig. 4, 70-80% of the maximum current amplitude remained 20 seconds after the peak response to 100 µM ACh. Similarly, frog α4β2 receptors depicted slow desensitisation profiles, with no significant differences when compared to that of rat ($p = 0.7326$) and chicken α4β2 ($p = 0.7204$) nAChRs (Table S8 and Fig. 4). The frog α7 nAChRs showed fast desensitisation with 2-3% of current remaining 5 seconds after the peak response to 1 mM ACh, similar to that of rat α7 ($p = 0.3743$) and chicken α7 ($p = 0.2496$) nAChRs (Table S8 and Fig. 4).

The conserved desensitisation profiles observed for both types of neuronal receptors was in stark contrast with that of α9α10 receptors. While rat and chicken α9α10 receptors showed similar and somewhat slow desensitization, with 60-65% of current remaining 20 seconds after the peak response to ACh ($p = 0.9999$), frog α9α10 nAChRs exhibited significantly higher desensitization when compared to rat α9α10 ($p=0.0051$) and chicken α9α10 ($p=0.0042$) receptors (Fig. 4 and Table S7).

Neuronal nAChRs are potentiated by extracellular divalent cations such as Ca^{2+} via an allosteric and voltage-independent mechanism (37, 38). The rat α9α10 nAChR, on the other hand, is both potentiated and blocked by physiological concentrations of extracellular divalent cations (39). Blockage occurs in the milimolar range, is voltage dependent and proposed to occur as a result of calcium permeation (39). To perform a comparative analysis of calcium modulation on rat, chicken and frog α4β2, α7 and α9α10 receptors, responses to near-EC_{50} concentrations of ACh were recorded in normal Ringer's solution at a range of Ca^{2+} concentrations and normalised to the response at 1.8 mM Ca^{2+}. For the neuronal α4β2 and α7 receptors from all three species, a similar potentiation pattern was observed, with increasingly higher responses to ACh at greater Ca^{2+} concentrations (Fig. 5 – top and middle panels). In contrast, responses of α9α10 nAChRs from rat, chicken and frog exhibited differential modulation by extracellular Ca^{2+}. As previously reported for the rat α9α10 receptor, responses to ACh were potentiated and blocked by extracellular Ca^{2+} (Fig. 5 - bottom left panel and (39)). The chicken α9α10 receptor also showed peak potentiation of the ACh response at 0.5 mM extracellular Ca^{2+}. However, no evident block was observed at higher concentrations of the cation (Fig. 5 - bottom middle panel). Finally, the frog α9α10 receptor showed potentiation of ACh responses at all Ca^{2+} concentrations assayed, with maximal responses detected at 3 mM Ca^{2+} (Fig. 5 - bottom right panel).

Calcium permeation through nAChRs holds great functional significance for the activation of calcium dependent conductances and intracellular signalling pathways (14). Receptors containing the α7 subunit have high calcium permeability (40) whereas receptors containing α4β2 subunits have a lower contribution of calcium to the total current (28, 41). Amniote inner ear hair cell α9α10 nAChRs show differences in the extent of calcium permeability (23, 28). In order to perform a comparative analysis of the extent of the calcium component of ACh responses, we studied the differential activation of the oocyte's endogenous calcium-activated chloride current ($I_{Cl_{Ca}}$). In oocytes expressing a recombinant receptor with high calcium permeability, the $I_{Cl_{Ca}}$ is strongly activated upon ACh application (42). Incubation of oocytes with the membrane-permeant fast Ca^{2+} chelator BAPTA-AM subsequently abolishes the Cl^- component of the total measured current (43). Fig. 6 shows representative responses to ACh before and after a 3-hour incubation with BAPTA-AM for α4β2, α7 and α9α10 nAChRs from rat, chicken and frog. Whereas ACh-evoked currents were only slightly affected in all α4β2 nAChRs denoting no major calcium influx (70-80% of current remaining after BAPTA incubation, Fig. 6, left panel), all α7 receptors showed a strong reduction of the ACh response after BAPTA incubation (30-40% of current remaining after BAPTA), indicating significant calcium permeation (Fig. 6, middle panel). Thus, no inter-species differences in the proportion of calcium current for both the low calcium permeant α4β2 and the highly calcium permeant α7

neuronal receptors were observed (Table S8). Conversely, and as previously reported (23, 28), we observed a marked difference in the extent of calcium current between the rat and chicken α9α10 receptors ($p = 0.0299$ – Fig. 6, right panels and Table S8). Moreover, the percentage of remaining response after BAPTA-AM incubation for the frog α9α10 receptor (Fig. 6, right panels) was similar to that of the rat receptor ($p = 0.9999$ – Table S8) and significantly different from that of the chicken α9α10 nAChR ($p = 0.0013$ – Table S8).

Neuronal nAChRs are characterised by a strong inward rectification, with negligible current at depolarized potentials (40, 41). This is proposed to be a relevant feature for their roles as pre-synaptic modulators of neuronal transmission (41). On the other hand, amniote α9α10 nAChRs exhibit a peculiar current-voltage (I-V) relationship due to a considerable outward current at positive potentials (19, 28). In order to perform a comparative analysis of the rectification profiles of neuronal and hair cell nAChRs we obtained I-V curves and determined the ratio of current elicited at +40 mV to that at -90 mV (I_{+40}/I_{-90}). All neuronal nAChRs exhibited I-V curves with marked inward rectification with no significant inter-species differences for either α4β2 or α7 tetrapod receptors, presenting I_{+40}/I_{-90} values below 1 (Fig. 7, left and middle panels and Table S8). On the contrary, each of the hair cell α9α10 nAChRs analysed presented a unique I-V profile. As previously reported, rat α9α10 receptors showed significant outward current at depolarised potentials and greater inward current at hyperpolarised potentials with a I_{+40}/I_{-90} ratio close to 1 (Fig. 7, right panels and (19)). The chicken α9α10 receptor showed outward current similar to that of the rat α9α10 receptor, but the inward current was smaller (Fig. 7, top right panel), resulting in a significantly higher I_{+40}/I_{-90} ratio ($p = 0.0229$ – Table S8). Surprisingly, the frog α9α10 receptor showed an I-V profile similar to that of neuronal nAChRs, with strong inward rectification, almost no outward current at depolarised potentials (Fig. 7, right panels) and a I_{+40}/I_{-90} below 1, significantly different to that obtained for chick ($p = 0.0406$ – Table S8) and rat ($p < 0.0001$ – Table S9) α9α10 receptors.

Comparative functional analysis of neuronal and hair cell nAChRs shows distinct evolutionary trajectories

Altogether, the characterisation of individual functional properties of tetrapod nAChRs showed a stark contrast between neuronal and hair cell nAChRs. In order to concomitantly analyse the diversification, or conservation of receptor function, we performed principal component analysis (PCA) on all the functional variables measured on α4β2, α7 and α9α10 receptors from the three species (Table S10). The first two principal components accounted for 82% of the variability (Fig. 8). Moreover, the distribution of receptors in PCA space reflected their overall functional differences and similarities. Both neuronal α4β2 and α7 receptors occupied distinct regions, more distant in PC1

than in PC2 denoting that these receptors differ more on ACh apparent affinity, desensitisation and calcium permeability than they do on rectification and calcium modulation (Fig. 8 - inset). Also, α4β2 and α7 receptors from the different species were located very close together, reflecting the lack of inter-species differences in functional properties. In contrast, the hair cell α9α10 receptors from the different species were distant from each other in PCA space, denoting their extensive functional divergence (Fig. 8). Interestingly, the frog α9α10 nAChR was closer to the α7 receptors than to its amniote counterparts, highlighting the overall functional similarity between the amphibian α9α10 and α7 nAChRs.

Amino acid sequence phylogenies, co-expression/co-assembly patterns and functional experiments support the hypothesis of differential evolutionary trajectories for neuronal and hair cell receptors. Further insight could be attained by the evaluation of the receptors present in the last common ancestor of rat and chicken (amniote ancestor) and of rat, chicken and frog (tetrapod ancestor). To tackle this, we inferred the character state for the functional properties of the α4β2, α7 and α9α10 ancestral receptors (see SI methods). We then projected this predicted functional states onto the functional PCA space of the extant receptors (Fig. 8). As expected, the predicted ancestral α4β2 and α7 amniote and tetrapod receptors were located close to their extant counterparts. In contrast, the predicted ancestral states of the α9α10 receptors were localised halfway between the frog α9α10 and the amniote chicken and rat α9α10 extant receptors, potentially reflecting the functional evolutionary trajectory of the hair cell receptor. Thus, the ancestral tetrapod α9α10 receptor may have functionally resembled the extant frog α9α10 receptor and neuronal α7 receptors, mainly on properties with heavier loading on PC2 (i.e., rectification and calcium permeability). Moreover, the ancestral amniote α9α10 receptor may have had functional properties that more closely resembled those of neuronal α4β2 receptors, in particular for properties with heavier loading on PC1 (i.e., ACh apparent affinity, desensitization and calcium modulation). In summary, the data portrayed in Fig. 8 describes a plausible scenario for the functional evolutionary trajectories undertaken by two neuronal and the hair cell nAChRs within the tetrapod lineage.

Discussion

The expansion of ion channel families on the vertebrate stem branch was mostly driven by two rounds of whole genome duplications (44). This has played a crucial role in the evolution of nervous systems and provided raw material that enabled the diversification of cell types (45) resulting in the complexity reached by vertebrate brains (e.g.(46)). Among the different ion channel families, Cys-loop receptors are within those that underwent the greatest expansion (45). The entire extant complement of nAChRs, which includes 17 different subunits (α1-α10, β1-β4, δ, ε and γ), was already present in the last common ancestor of all vertebrates (10). With the exception of some fish species that acquired α11, β1.2 and β5 subunits, for which no expression or functional data has yet been reported (10), and the loss of the α7-like α8 subunits in mammals, the complement of original vertebrate nAChR subunits has been remarkably conserved. Moreover, nAChRs are unique in that subgroups of the family have distinct roles in synaptic transmission in non-overlapping domains, either in the nervous system, inner ear hair cells or the neuromuscular junction (13, 14, 18). In this work, we performed in-depth analyses of coding sequence molecular evolution, subunit co-expression patterns and comparative functional properties of neuronal and hair cell receptors to explore the potential impact of these segregation of nAChRs subgroups on their respective evolutionary histories. We found that neuronal subunits showed high degree of coding sequence conservation, coupled to greater co-expression variability and conservation of functional properties across tetrapod clades. In contrast, the hair cell α9α10 nAChR showed greater sequence divergence, a highly restricted co-expression pattern and a great degree of variability of functional properties across species. These results indicate that along the tetrapod lineage neuronal and hair cell nAChRs underwent alternative evolutionary trajectories.

Functional conservation of neuronal nAChRs

The observation that the biophysical functional properties of neuronal α4β2 and α7 nAChRs were conserved in the three tetrapod species analysed, relates to their high degree of amino acid sequence conservation (Fig. 1 and Tables S2-S3). Cholinergic innervation is pervasive, with almost every area of the brain being influenced by nicotinic signalling (14). Moreover, the expression of neuronal nAChR subunits is widespread in the central and peripheral nervous system (Fig. 2), where they assemble in multiple combinations (Table S6). Thus, randomly acquired changes in the coding sequence of a given subunit might be deleterious for receptor function in a multitude of heteropentameric assemblies present in diverse neuronal types. Such changes would therefore be under strong negative selection pressure. This is in agreement with the low degree of divergence observed for neuronal subunits and the absence of signatures of positive selection in the protein-

344 coding sequences of α4, β2 and α7 subunits (28) and other brain expressed genes (47). However,
345 neurons could alternatively resort to re-shuffling of the complement of nAChR subunits being
346 expressed to attain functional divergence. Therefore, and as for most brain expressed genes (47, 48),
347 random changes in non-coding regions that lead to differential expression patterns across brain
348 areas or species may have played a substantial role in delineating the evolutionary trajectories of
349 neuronal nAChRs.

350 *Differential co-expression patterns of neuronal and hair cell nAChRs*

351 Our meta-analysis of expression patterns across the mouse brain highlights numerous instances of
352 potential functional variability and diversification, even between closely related neuronal types (Fig.
353 2, S4-S6). For instance, cholinergic input controls dopaminergic neuron firing patterns in the
354 midbrain (49). Here co-expression of nAChR subunits greatly differs across the four subtypes of
355 dopaminergic neurons in the ventral tegmental area (VTA) ((50) and Fig. 2), indicating that they may
356 express differential levels of functionally distinct α4β2 containing (α4β2*) receptors. Inclusion of the
357 α5 subunit can alter α4β2* receptor properties substantially, increasing ACh sensitivity,
358 desensitization kinetics and Ca^{2+} permeability (51-53). In addition, incorporation of the β3 subunit to
359 the α4β2* receptor also increases ACh sensitivity, without significantly affecting Ca^{2+} permeability
360 (51, 53). Moreover, VTA dopaminergic neurons also showed expression of the α6 and α3 subunits,
361 both of which can co-assemble with α4, α5 and/or β2 subunits, greatly enhancing the complexity of
362 individual nAChRs-mediated responses of VTA dopaminergic neurons to modulatory cholinergic
363 input. Another interesting example is provided by layer VI cortical pyramidal neurons, whose activity
364 is modulated by a dense cholinergic innervation from the basal forebrain. Here, ACh elicits robust
365 excitatory responses acting on α4β2* nAChRs, with layer VI being one of the few cortical areas that
366 express the accessory α5 nAChR subunit (54). Cortical neurons that project to both the ventral
367 posteromedial nucleus (VPM) and the posteromedial complex of the thalamus express significantly
368 higher levels of the α5 subunit than neurons projecting to the VPM only (Fig. S6A). This suggests
369 VPM-only projecting neurons could have a lower density of α4α5β2 compared to α4β2 nAChRs,
370 potentially contributing to differential cholinergic modulation of these subtypes of layer VI neurons,
371 that also show differences in excitability (55).

372 Hair cells of the inner ear express high levels of α9 and α10 subunits, along with a number of
373 neuronal (β2 and β4) and muscle (α1, β1, γ/ε) subunits (Fig. 2 and (20, 56)). α9α10 nAChRs mediate
374 fast efferent neurotransmission to cochlear and vestibular hair cells in the inner ear (13) and are
375 characterised by unique pharmacological and biophysical properties (19, 22, 39, 57). Most notably,
376 nicotine, the diagnostic agonist of the nAChRs family, does not act as an agonist of α9α10 receptors,

but as a competitive antagonist (19). In inner ear hair cells, no responses to nicotine application are detected (20, 58), indicating that functional muscle or neuronal nAChRs are not present at the plasma membrane. The presence of neuronal and muscle subunits mRNA may result from redundant or residual transcriptional regulation mechanisms. Moreover, similar "leaky" expression of muscle subunits was detected in a number of neuronal types (Fig. 2).

Expression of α9 and α10 subunit is restricted to inner ear hair cells, with a few interesting exceptions. In the inner ear, spiral ganglion neurons (SGNs) provide afferent innervation to cochlear hair cells and express a range of neuronal nAChR subunits (Fig. 2 and (59, 60)). Interestingly, low levels of α9 and α10 subunits are present in SGNs (Fig. 2 and (61)) with similarly low co-expression detected by two independent single-cell RNA sequencing studies (62, 63). If this low level of α9 and α10 mRNA proves to be more than "transcriptional noise", then SGNs may be unique among neurons in expressing the hair cell α9α10 receptor. This might be related to the shared developmental origin of SGNs and hair cells at the otic placode (64, 65) and could open the possibility that in addition to neuronal nAChRs, which are thought to partly mediate the nicotinic effect of lateral olivocochlear terminals on afferent dendrites (66), α9α10 nAChRs may also play a role. Finally, in dorsal root ganglia neurons, α9 expression was not detected, while α10 is present at very low levels in only a few subtypes (Fig. 2 and (67)). These observations support those reported by qPCR and functional assays (68) and provide further evidence that the participation of α9* nAChRs in pain processes is not due to its presence in dorsal root ganglia neurons (68, 69).

Of note, α9 and α10, together with other nAChR subunits, are expressed in other peripheral, non-neuronal, tissues (17, 70). A plausible autocrine/paracrine effect of ACh in these cells can be served by a multiple and redundant battery of nAChRs that might play a signalling function in these peripheral tissues (71, 72). Due to the redundancy in pathways for ACh signalling, it is unlikely that the function of α9α10 nAChRs in these peripheral tissues provided the selection forces that shaped the accumulation of non-synonymous changes on this receptor.

The α9α10 nAChR and the evolution of the efferent olivocochlear system

The observations that α9 and α10 genes are only co-ordinately transcribed in inner ear hair cells, together with their ability to only form functional heteromeric receptors when co-assembled with each other but not with other nAChR subunits (19, 20, 22), support our hypothesis that evolutionary changes in the hair cell receptors may have been focused at the coding sequence. Accordingly, vertebrate α9 and α10 subunits exhibit significant sequence divergence (Table S3 and Fig. 1), with mammalian α10 subunits showing a higher than expected accumulation of non-synonymous substitutions that were positively selected (26, 28). In addition, both α9 and a10 subunits show a

high number of clade-specific (mammalian vs sauropsid) functionally relevant aminoacid changes (Fig. 1, Table S3 and (23)). Consequently, the biophysical properties of α9α10 receptors drastically changed across vertebrate species (Fig. 8 and (23, 28)). Since the primary function of the α9α10 receptor is at the postsynaptic side of the olivocochlear synapse, it can be hypothesised that clade specific differences in efferent modulation of hair cell activity could have shaped the functional properties of α9α10 receptors. Upon the transition to land, the hearing organs of tetrapods underwent parallel evolutionary processes, mainly due to the independent emergence of the tympanic middle ear, at least five times, in separate groups of amniotes (73). This was followed by the independent elongation of the auditory sensory epithelia that extended the hearing range to higher frequencies and the elaboration of passive and active sound amplification mechanisms that lead to the fine tuning of sound detection (73, 74). More importantly, mammals and sauropsids underwent a parallel diversification of hair cell types, segregating, partially in birds but completely in mammals, the phonoreception and sound amplification functions (75). Efferent innervation to hair cells, mediated by α9α10 nAChRs, is an ancestral feature common to all vertebrate species (76). In the auditory epithelia it modulates sound amplification and followed the hair cell diversification pattern: in birds it mainly targets short hair cells, while in mammals it targets outer hair cells (75). The latter developed a clade-specific sound amplification mechanism driven by the motor protein prestin and termed somatic electromotility (74). Prestin, together with βV giant spectrin, a major component of the outer hair cells' cortical cytoskeleton which is necessary for electromotility, show signatures of positive selection in the mammalian clade that may relate to the acquisition of somatic electromotility (26, 77). Thus, the mammalian clade-specific evolutionary processes observed in both the α9 and α10 subunits (23, 26, 28) may be related to overall changes in the efferent olivovochlear systems of this clade that is tasked with the modulation of prestin-driven somatic electromotility. A recent high throughput evolutionary analysis identified 167 inner ear expressed genes with signatures of positive selection in the mammalian lineage (78). These inner ear genes, including those encoding the α9 and α10 nAChR subunits, can be considered as hotspots for evolutionary innovation in the auditory system across species.

Such a scenario provides a context for evaluating the relationship between evolutionary trajectories and the functional role of α9α10 receptors. In mammals, the high calcium influx through α9α10 receptors activates large conductance, voltage and low-calcium-sensitive BK potassium channels mediating hyperpolarization of outer hair cells in higher frequency regions of the cochlea (79). In contrast, in short hair cells from the chicken basilar papillae, hyperpolarization is served by the ACh-dependent activation of high calcium sensitive SK potassium channels (80, 81). Moreover, in contrast to adult mammalian hair cells where efferent fibres directly contact outer hair cells, but not the

444 inner hair cells that release glutamate to activate afferent auditory fibres, efferent innervation in
445 birds and amphibians co-exists with afferent innervation in the same hair cells. Calcium influx in
446 these hair cells could therefore result in efferent-triggered, ACh-mediated release of glutamate to
447 auditory afferents due to calcium spill over, bypassing sound mechanotransduction. Thus, limiting
448 the extent of calcium influx through α9α10 nAChRs may be paramount to avoid confounding sensory
449 inputs. In this hypothetical scenario, the low calcium permeability of the avian α9α10 nAChR or the
450 very high desensitization kinetics of the amphibian α9α10 nAChR that restrict calcium load could be
451 related to the aforementioned selection pressure.

452 *Subgroups of nAChRs and differential sources of functional divergence*

453 Our observations on expression pattern, coding sequence and functional divergence support the
454 notion that α9 and α10 are not a subtype of brain nicotinic subunit (for review see (25)), but form a
455 group of their own, characterised by unique expression profile, pharmacological and biophysical
456 properties (19, 22, 39, 57) and evolutionary history.

457 The contrasting evolutionary trajectories of neuronal and hair cell receptors, with functional
458 variability stemming from combinatorial co-expression for the former and changes in coding
459 sequence for the latter, support the notion of differential substrates for random change and ensuing
460 functional divergence. For neuronal subunits, the source of random variability may have been
461 rooted on changes in regulatory sequences. In contrast, for the hair cell receptor, random changes in
462 the coding sequence were fixed throughout the evolutionary history of the tetrapod lineage.
463 Interestingly, muscle subunits showed relatively low levels of coding sequence conservation (Fig. 1)
464 and, via combinatorial co-assembly, muscle cells can toggle between at least two receptor variants
465 (18). This places muscle receptors in between the two extremes of hair cell (isolated) and neuronal
466 (widespread) receptors. A comparative functional study of muscle receptors would further test our
467 hypothesis, with the prediction that a modest level of functional divergence may be encountered,
468 but outweighed by the functional differences between muscle receptor variants.

469 In summary, the present work provides evidence supporting different evolutionary trajectories for
470 neuronal and hair cell nAChRs. These may have resulted from the differential substrates for random
471 change that dominated evolutionary processes in each receptor subgroup: diversity of co-
472 expression/co-assembly patterns for neuronal subunits, changes in coding sequence for hair cell
473 subunits. It results salient that among ligand-gated ion channels these alternative evolutionary
474 trajectories are a particular feature of the nAChRs family of Cys-loop receptors. Thus, this is not
475 observed for ionotropic glutamate and $GABA_A$ receptors, whose 18 (82) and 19 (83) member
476 subunits, respectively, are all expressed in the central nervous system. Finally, the simultaneous

477 analysing of coding sequences, expression patterns and protein functional properties generated new
478 insights into the evolutionary history of gene paralogues, thus providing further context for the role
479 of nAChRs in neuronal and hair cell synaptic transmission.

480

Methods

All experimental protocols were carried out in accordance with the guides for the care and use of laboratory animals of the National Institutes of Health and the Institutional Animal Care and Use Committee of the Instituto de Investigaciones en Ingeniería Genética y Biología Molecular, "Dr. Héctor N. Torres".

Phylogenetic analysis of vertebrate nAChRs subunits

All sequences were downloaded from GenBank (www.ncbi.nlm.nih.gov/genbank), UCSC (http://genome.ucsc.edu/) and Ensembl (www.ensembl.org) databases. Sequence alignment was performed using *Clustal*W on the MEGA7 software (84). Phylogenetic trees were inferred using the minimum evolution method (85). A detailed description of the alignment procedures, sequence identity analysis and phylogeny constructions are available in SI Methods.

Functional divergence analysis

The coefficient of type II functional divergence (θ_{II}), its standard error and the site-specific posterior probabilities were calculated for each nicotinic subunit between the mammalian and sauropsid clades using DIVERGE 3.0 (31). A detailed description of the analysis strategy is available in SI methods.

Analysis of nAChR subunit expression in single-cell RNAseq (scRNAseq) datasets

A meta-analysis of single cell gene expression data from 10 studies was performed to describe the expression patterns of nAChR subunits across cell types. Probability distributions of mean expression level for all nAChR subunit genes detected in all the cell types analysed were obtained using the *scde* package (32). We combined this with a comprehensive catalogue of experimentally validated subunit combinations and identified the subunit combinations that were present, in each cell type or absent all together. A detailed description of the datasets used and analysis strategy is available in SI methods.

Expression of recombinant receptors in Xenopus laevis oocytes and electrophysiological recordings

The plasmids used for heterologous expression in *Xenopus laevis* oocytes are described in SI Methods. Electrophysiological recordings from *Xenopus laevis* oocytes were obtained as described previously (22, 57) and are described in more detail in SI Methods. A detailed description of the protocols used to evaluate nAChR functional properties and statistical analysis is available in SI methods.

512 **Principal component analysis of functional properties and inference of character state of**
513 **functional properties of ancestral receptors**

514 Principal Component Analysis was performed on the experimental values obtained for the functional
515 properties of extant nAChRs implementing custom routines written in R v3.4.1 and run in RStudio
516 software v1.0.153 (see SI methods). The pipeline for the inference of the ancestral character state of
517 biophysical properties is described in detail in SI methods. Briefly, sequences corresponding to the
518 amniote and tetrapod ancestors were reconstructed for the different subunits. Distances were then
519 used to compute branch lengths on receptor trees. The latter, together with the biophysical
520 properties of extant receptors were used to infer the properties of ancestral receptors using the APE
521 package v5.2 (86). Finally, these were projected onto the PCA space of extant receptors.

522

Acknowledgments

This work was supported by Agencia Nacional de Promoción Científicas y Técnicas, Argentina, the Scientific Grand Prize of the Fondation Pour l'Audition and NIH Grant R01 DC001508 (Paul Fuchs PI and ABE co-PI) to ABE.

References

1. Dent JA (2006) Evidence for a diverse Cys-loop ligand-gated ion channel superfamily in early bilateria. *Journal of Molecular Evolution* 62(5):523-535.
2. Jaiteh M, Taly A, & Hénin J (2016) Evolution of pentameric ligand-gated ion channels: Pro-loop receptors. *PLoS ONE* 11(3):1-24.
3. Tasneem A, Iyer LM, Jakobsson E, & Aravind L (2005) Identification of the prokaryotic ligand-gated ion channels and their implications for the mechanisms and origins of animal Cys-loop ion channels. *Genome biology* 6(1):R4-R4.
4. Cully DF*, et al.* (1994) Cloning of an avermectin-sensitive glutamate-gated chloride channel from Caenorhabditis elegans. *Nature* 371(6499):707-711.
5. Hervé Thany S (2010) *Insect Nicotinic Acetylcholine Receptors* pp 1323-1330.
6. Hilf RJC & Dutzler R (2009) Structure of a potentially open state of a proton-activated pentameric ligand-gated ion channel. *Nature* 457(7225):115-118.
7. Karlin A (2002) Ion channel structure: Emerging structure of the Nicotinic Acetylcholine receptors. *Nature Reviews Neuroscience* 3(2):102-114.
8. Spurny R*, et al.* (2012) Pentameric ligand-gated ion channel ELIC is activated by GABA and modulated by benzodiazepines. *Proc.Natl.Acad.Sci.U.S.A.* 109(44):3028-3034.
9. Corringer PJ*, et al.* (2012) Structure and pharmacology of pentameric receptor channels: From bacteria to brain. *Structure* 20(6):941-956.
10. Pedersen JE, Bergqvist CA, & Larhammar D (2019) Evolution of vertebrate nicotinic acetylcholine receptors. *BMC Evolutionary Biology* 19(1):1-21.
11. Kalamida D*, et al.* (2007) Muscle and neuronal nicotinic acetylcholine receptors: Structure, function and pathogenicity. *FEBS Journal* 274(15):3799-3845.
12. Steinbach JH (1989) Structural and functional diversity in vertebrate skeletal muscle nicotinic acetylcholine receptors. *Ann Rev Physiol* (51):353-365.
13. Elgoyhen AB & Katz E (2012) The efferent medial olivocochlear-hair cell synapse. *Journal of Physiology Paris* 106(1-2):47-56.
14. Dani JA & Bertrand D (2007) Nicotinic Acetylcholine Receptors and Nicotinic Cholinergic Mechanisms of the Central Nervous System. *Annu. Rev. Pharmacol. Toxicol* 47:699-729.
15. Zoli M, Pistillo F, & Gotti C (2015) Diversity of native nicotinic receptor subtypes in mammalian brain. *Neuropharmacology* 96(PB):302-311.
16. Millar NS & Gotti C (2009) Diversity of vertebrate nicotinic acetylcholine receptors. *Neuropharmacology* 56(1):237-246.
17. Zoli M, Pucci S, Vilella A, & Gotti C (2018) Neuronal and Extraneuronal Nicotinic Acetylcholine Receptors. *Current neuropharmacology* 16(4):338-349.
18. Mishina M*, et al.* (1986) Molecular distinction between fetal and adult forms of muscle acetylcholine receptor. *Nature* 321(6068):406-411.
19. Elgoyhen AB*, et al.* (2001) α10: a Determinant of Nicotinic Cholinergic Receptor Function in Mammalian Vestibular and Cochlear Mechanosensory Hair Cells. *Proc.Natl.Acad.Sci.U.S.A.* 98(6):3501-3506.
20. Scheffer D*, et al.* (2007) The α1 subunit of nicotinic acetylcholine receptors in the inner ear: transcriptional regulation by ATOH1 and co-expression with the γ subunit in hair cells. *Journal of Neurochemistry* 0(0):071027034430002--???
21. Sgard F*, et al.* (2002) A novel human nicotinic receptor subunit, alpha10, that confers functionality to the alpha9-subunit. *Molecular Pharmacology* 61(1):150-159.
22. Elgoyhen AB, Johnson DS, Boulter J, Vetter DE, & Heinemann S (1994) α9: an acetylcholine receptor with novel pharmacological properties expressed in rat cochlear hair cells. *Cell* 79(4):705-715.
23. Lipovsek M*, et al.* (2014) Tracking the molecular evolution of calcium permeability in a nicotinic acetylcholine receptor. *Mol Biol Evol* 31(12):3250-3265.

24. Vetter DE*, et al.* (2007) The a10 nicotinic acetylcholine receptor subunit is required for normal synaptic function and integrity of the olivocochlear system. *Proc.Natl.Acad.Sci.U.S.A.* 104(51):20594-20599.
25. Morley BJ, Whiteaker P, & Elgoyhen AB (2018) Commentary: Nicotinic Acetylcholine Receptor α9 and α10 Subunits Are Expressed in the Brain of Mice. *Frontiers in Cellular Neuroscience* 12(May):10-13.
26. Franchini LF & Elgoyhen AB (2006) Adaptive evolution in mammalian proteins involved in cochlear outer hair cell electromotility. *Molecular Phylogenetics and Evolution* 41(3):622-635.
27. Le Novère N, Corringer P-J, & Changeux J-P (2002) The diversity of subunit composition in nAChRs: evolutionary origins, physiologic and pharmacologic consequences. *Journal of neurobiology* 53(4):447-456.
28. Lipovsek M*, et al.* (2012) Phylogenetic differences in calcium permeability of the auditory hair cell cholinergic nicotinic receptor. *Proc.Natl.Acad.Sci.U.S.A.* 109(11):4308-4313.
29. Ortells M & Lunt GG (1995) History of the Ligand-Gated Superfamily of Receptors. *Trends neuroscience* 18(3):121-127.
30. Tsunoyama K & Gojobori T (1998) Evolution of Nicotinic Acetylcholine Receptor Subunits. *Mol Biol Evol* 15(5):518-527.
31. Gu X*, et al.* (2013) An update of DIVERGE software for functional divergence analysis of protein family. *Mol Biol Evol* 30(7):1713-1719.
32. Kharchenko PV, Silberstein L, & Scadden DT (2014) Bayesian approach to single-cell differential expression analysis. *Nature Methods* 11(7):740-742.
33. Chevée M, Robertson JDJ, Cannon GH, Brown SP, & Goff LA (2018) Variation in Activity State, Axonal Projection, and Position Define the Transcriptional Identity of Individual Neocortical Projection Neurons. *Cell Reports* 22(2):441-455.
34. Moroni M, Zwart R, Sher E, Cassels BK, & Bermudez I (2006) α4β2 Nicotinic receptors with high and low acetylcholine sensitivity: Pharmacology, stoichiometry, and sensitivity to long-term exposure to nicotine. *Mol Pharmacol.* 70(2):755-768.
35. Quick MW & Lester RAJ (2002) Desensitization of neuronal nicotinic receptors. *Journal of Neurobiology* 53(4):457-478.
36. Mazzaferro S, Bermudez I, & Sine SM (2017) α4β2 Nicotinic Acetylcholine Receptors: Relationship between subunit stoichiometry and function at the single channel level. *The Journal of biological chemistry* 292(7):2729-2740.
37. Mulle C, Léna C, & Changeux JP (1992) Potentiation of nicotinic receptor response by external calcium in rat central neurons. *Neuron* 8(5):937-945.
38. Vernino S, Amador M, Luetje CW, Patrick J, & Dani JA (1992) Calcium modulation and high calcium permeability of neuronal nicotinic acetylcholine receptors. *Neuron* 8(1):127-134.
39. Weisstaub N, Vetter DE, Elgoyhen AB, & Katz E (2002) The α9α10 nicotinic acetylcholine receptor is permeable to and is modulated by divalent cations. *Hearing Research* 167(1-2):122-135.
40. Séguéla P, Wadiche J, Dineley-Miller K, Dani JA, & Patrick JW (1993) Molecular cloning, functional properties, and distribution of rat brain alpha 7: a nicotinic cation channel highly permeable to calcium. *J Neuroscience* 13(2):596-604.
41. Haghighi AP & Cooper E (2000) A molecular link between inward rectification and calcium permeability of neuronal nicotinic acetylcholine α3β4 and α4β2 receptors. *J Neuroscience* 20(2):529-541.
42. Barish ME (1983) A transient calcium-dependent choloride current in the immature Xenopus oocytes. *J Physiol* 342:309-325.
43. Gerzanich V, Anand R, & Lindstrom JM (1994) Homomers of α8 and α7 subunits of nicotinic receptors exhibit similar channel but contrasting binding site properties. *Molecular Pharmacology* 45(2):212 LP-- 220.

44. Roux J, Liu J, & Robinson-Rechavi M (2017) Selective constraints on coding sequences of nervous system genes are a major determinant of duplicate gene retention in vertebrates. *Mol Biol Evol* 34(11):2773-2791.
45. Liebeskind BJ, Hillis DM, & Zakon HH (2015) Convergence of ion channel genome content in early animal evolution. *Proc.Natl.Acad.Sci.U.S.A.* 112(8):E846--E851.
46. Sugino K*, et al.* (2019) Mapping the transcriptional diversity of genetically and anatomically defined cell populations in the mouse brain. *eLife* 8.
47. Haygood R, Babbitt CC, Fedrigo O, & Wray GA (2010) Contrasts between adaptive coding and noncoding changes during human evolution. *Proc.Natl.Acad.Sci.U.S.A.* 107(17):7853-7857.
48. Hoekstra HE & Coyne JA (2007) The locus of evolution: evo devo and the genetics of adaptation. *Evolution* 61(5):995-1016.
49. Mameli-Engvall M*, et al.* (2006) Hierarchical Control of Dopamine Neuron-Firing Patterns by Nicotinic Receptors. *Neuron* 50(6):911-921.
50. La Manno G*, et al.* (2016) Molecular diversity of midbrain development in resource molecular diversity of midbrain development in mouse, human and stem cells. *Cell* 167:566-580.
51. Kuryatov A, Onksen J, & Lindstrom J (2008) Roles of accessory subunits in alpha4beta2(*) nicotinic receptors. *Molecular Pharmacology* 74(1):132-143.
52. Ramirez-Latorre J*, et al.* (1996) Functional contributions of α5 subunit to neuronal acetylcholine receptor channels. *Nature* 380(6572):347-351.
53. Tapia L, Kuryatov A, & Lindstrom J (2007) Ca2+ Permeability of the (α4)3(β2)2 Stoichiometry Greatly Exceeds That of (α4)2(β2)3 Human Acetylcholine Receptors. *Molecular Pharmacology* 71(3):769-776.
54. Proulx E, Piva M, Tian MK, Bailey CDC, & Lambe EK (2014) Nicotinic acetylcholine receptors in attention circuitry: The role of layer VI neurons of prefrontal cortex. *Cellular and Molecular Life Sciences* 71(7):1225-1244.
55. Landisman CE & Connors BW (2007) VPM and PoM nuclei of the rat somatosensory thalamus: Intrinsic neuronal properties and corticothalamic feedback. *Cerebral Cortex* 17(12):2853-2865.
56. Roux I, Wu JS, McIntosh JM, & Glowatzki E (2016) Assessment of the expression and role of the α1 -nAChR subunit in efferent cholinergic function during the development of the mammalian cochlea. *Journal of Neurophysiology* 116(2):479-492.
57. Katz E*, et al.* (2000) High calcium permeability and calcium block of the α9 nicotinic acetylcholine receptor. *Hearing Research* 141:117-128.
58. Gomez-Casati ME, Fuchs PA, Elgoyhen AB, & Katz E (2005) Biophysical and pharmacological characterization of nicotinic cholinergic receptors in rat cochlear inner hair cells. *J Physiol* 566(Pt 1):103-118.
59. Hiel H, Elgoyhen AB, Drescher DG, & Morley BJ (1996) Expression of nicotinic acetylcholine receptor mRNA in the adult rat peripheral vestibular system. *Brain Research* 738(2):347-352.
60. Morley BJ, Li HS, Hiel H, Drescher DG, & Elgoyhen AB (1998) Identification of the subunits of the nicotinic cholinergic receptors in the rat cochlea using RT-PCR and in situ hybridization. *Molecular Brain Research* 53(1-2):78-87.
61. Shrestha BR*, et al.* (2018) Sensory neuron diversity in the inner ear is shaped by activity sensory neuron diversity. *Cell* 174:1229-1246.
62. Sun S*, et al.* (2018) Hair Cell Mechanotransduction Regulates Spontaneous Activity and Spiral Ganglion Subtype Specification in the Auditory System. *Cell* 174(5):1247-1263 e1215.
63. Petitpre C*, et al.* (2018) Neuronal heterogeneity and stereotyped connectivity in the auditory afferent system. *Nature Communications* 9(1):3691.
64. Arendt D*, et al.* (2016) The origin and evolution of cell types. *Nature reviews. Genetics* 17(12):744-757.

65. Fritzsch B & Beisel KW (2004) Keeping sensory cells and evolving neurons to connect them to the brain: molecular conservation and novelties in vertebrate ear development. *Brain, Behavior and Evolution* 64(3):182-197.
66. Reijntjes DOJ & Pyott SJ (2016) The afferent signaling complex: Regulation of type I spiral ganglion neuron responses in the auditory periphery. *Hearing Research* 336:1-16.
67. Usoskin D*, et al.* (2015) Unbiased classification of sensory neuron types by large-scale single-cell RNA sequencing. *Nature Neuroscience* 18(1):145-153.
68. Hone AJ, Meyer EL, McIntyre M, & McIntosh JM (2011) Nicotinic acetylcholine receptors in dorsal root ganglion neurons include the α6β4* subtype. *The FASEB Journal* 26(2):917-926.
69. Rau KK, Johnson RD, & Cooper BY (2004) Nicotinic AChR in Subclassified Capsaicin-Sensitive and -Insensitive Nociceptors of the Rat DRG. *Journal of Neurophysiology* 93(3):1358-1371.
70. McIntosh JM, Absalom N, Chebib M, Elgoyhen AB, & Vincler M (2009) Alpha9 nicotinic acetylcholine receptors and the treatment of pain. *Biochemical Pharmacology* 78(7):693-702.
71. Zakrzewicz A*, et al.* (2017) Canonical and Novel Non-Canonical Cholinergic Agonists Inhibit ATP-Induced Release of Monocytic Interleukin-1beta via Different Combinations of Nicotinic Acetylcholine Receptor Subunits alpha7, alpha9 and alpha10. *Frontiers in Cellular Neuroscience* 11:189.
72. Criado M (2018) Acetylcholine nicotinic receptor subtypes in chromaffin cells. *Pflugers Archiv : European journal of physiology* 470(1):13-20.
73. Manley GA (2017) Comparative Auditory Neuroscience: Understanding the Evolution and Function of Ears. *Journal of the Association for Research in Otolaryngology : JARO* 18(1):1-24.
74. Dallos P (2008) Cochlear amplification, outer hair cells and prestin. *Current opinion in neurobiology* 18(4):370-376.
75. Koppl C (2011) Birds--same thing, but different? Convergent evolution in the avian and mammalian auditory systems provides informative comparative models. *Hearing Research* 273(1-2):65-71.
76. Sienknecht UJ, Köppl C, & Fritzsch B (2014) Evolution and development of hair cell polarity and efferent function in the inner ear. *Brain, Behavior and Evolution* 83(2):150-161.
77. Cortese M*, et al.* (2017) Spectrin βV adaptive mutations and changes in subcellular location correlate with emergence of hair cell electromotility in mammalians. *Proc.Natl.Acad.Sci.U.S.A.* 114(8):2054-2059.
78. Pisciottano F, Cinalli AR, Stopiello M, & Castagna VC (2019) Positive Selection and Adaptation of Novel Inner Ear Genes in the Mammalian Lineage. *Mol Biol Evol*.
79. Wersinger E, McLean WJ, Fuchs PA, & Pyott SJ (2010) BK Channels Mediate Cholinergic Inhibition of High Frequency Cochlear Hair Cells. *PLoS ONE* 5(11):e13836-e13836.
80. Fuchs PA & Murrow B (1992) Cholinergic inhibition of short (outer) hair cells of the chick's cochlea. *J Neuroscience* 12(3):800-809.
81. Samaranayake H, Saunders JC, Greene MI, & Navaratnam DS (2004) Ca2+ and K+ (BK) channels in chick hair cells are clustered and colocalized with apical-basal and tonotopic gradients. *J Physiol* 560(1):13-20.
82. Traynelis SF*, et al.* (2010) Glutamate receptor ion channels: Structure, regulation, and function. *Pharmacological Reviews* 62(3):405-496.
83. Tsang SY, Ng SK, Xu Z, & Xue H (2007) The evolution of GABAA receptor-like genes. *Mol Biol Evol* 24(2):599-610.
84. Kumar S, Stecher G, & Tamura K (2016) MEGA7: Molecular Evolutionary Genetics Analysis Version 7.0 for Bigger Datasets. *Mol Biol Evol* 33(7):1870-1874.
85. Rzhetsky A & Nei M (1992) A simple method for estimating and testing minimum-evolution trees. *Mol Biol Evol* 9(5):945-967.
86. Paradis E, Claude J, & Strimmer K (2004) APE: Analyses of phylogenetics and evolution in R language. *Bioinformatics* 20(2):289-290.

730

731

732

Figure legends

Figure 1. Hair cell nAChR subunits show greater sequence divergence than neuronal subunits. A. Phylogenetic relationships between vertebrate nicotinic subunits. The branches corresponding to the same subunits of different species were collapsed up to the node at which one subunit separates from its closest neighbour. The complete tree is shown in Fig. S1. Triangles length denotes the divergence on sequence identity from the subunit node. Triangles were coloured according to the average percentage of sequence identity between all pairs of sequences (%seqID, Table S2) within the branch. Numbers in branches indicate the bootstrap value obtained after 1,000 replicates. Scale bar indicates the number of amino acid substitutions per site. B. Posterior probabilities for type II functional divergence between mammalian and sauropsid clades, for each site along individual nAChR subunits. Grey lines, posterior probability ≤ 0.65. Red lines, posterior probability < 0.65. Bottom right, diagram of a nAChR subunit extracellular, 4 transmembrane and intracellular domains along aminoacid position.

Figure 2. Hair cell nAChR subunits are co-expressed in inner ear hair cells, while neuronal subunits show widespread and variable co-expression patterns. Normalised mean expression level for nAChR subunits across mouse neuronal and sensory cell types. Circle sizes indicate the mean expression level for each cell type, normalised to the highest value observed within each dataset. For detailed explanations of individual cell types refer to main text, SI methods section or the original publications.

Figure 3. Hair cell nAChRs show differences in ACh apparent affinity, while neuronal nAChRs have similar ACh sensitivity. **A.** Concentration-response curves for neuronal α4β2 and α7 nAChRs and hair cell α9α10 nAChRs from three tetrapod species. Values are mean ± S.E.M. Lines are best fit to the Hill equation (n = 4-9). Representative responses evoked by 10 μM (α4β2, rat and chick α9α10) or 100 μM (α7, frog α9α10) ACh are shown next to their respective plots. Scale bars: α4β2: 100 nA, 10 sec; α7: 50 nA, 5 sec; α9α10: 50 nA, 10 sec. **B.** Representative responses evoked by ACh in oocytes injected with rat, chicken or frog homomeric α9 and α10 subunits (n=2–20).

Figure 4. Hair cell nAChRs differ in their desensitization patterns, while neuronal receptors show similar profiles. *Top panels*. Representative responses of α4β2, α7 and α9α10 nAChRs to a 60 seconds (for α4β2 and α9α10) or 30 seconds (for α7) application of 100 μM ACh for all α4β2 and amniotes α9α10, and 1 mM ACh for all α7 and frog α9α10 nAChRs. *Bottom panels*. Percentage of current remaining 20 seconds (α9α10 and α4β2) or 5 seconds (α7) after the peak response, relative to the maximum current amplitude elicited by ACh. Bars represent mean ± S.E.M., open circles

represent individual oocytes (n = 4-10). **p<0.01, One-Way ANOVA followed by Dunn's test (α4β2 nAChRs) or Kruskal-Wallis followed by Holm Sidak's test (α7 and α9α10 nAChRs).

Figure 5. Extracellular Ca^{2+} potentiates neuronal nAChRs but differentially modulates α9α10 nAChRs. ACh response amplitude as a function of extracellular Ca^{2+} concentration. ACh was applied at near-EC50 concentrations (10 µM ACh for all α4β2, rat and chick α9α10 nAChRs and 100 µM ACh for all α7 and frog α9α10 nAChRs). Current amplitudes recorded at different Ca^{2+} concentrations in each oocyte were normalized to the response obtained at 1.8 mM Ca^{2+} in the same oocyte. V_h: -90 mV. Bars represent mean ± S.E.M., open circles represent individual oocytes (n = 4-12). *p<0.05, **p<0.01, ***p<0.005, ****p<0.0001, Paired *t*-test (rat and frog α4β2 nAChRs and all α7 and α9α10 nAChRs) or Wilcoxon matched pair test (chick α4β2 nAChR) – comparing 0.5 mM Ca^{2+} vs 3 mM Ca^{2+}.

Figure 6. Unlike neuronal nAChRs, α9α10 nAChRs exhibit differential Ca^{2+} contribution to the total inward current. *Top panels*. Representative responses to near-EC_{50} concentration of ACh (10 µM ACh for all α4β2 and amniotes α9α10 nAChRs and 100 µM ACh for all α7 and frog α9α10 nAChRs) in oocytes expressing α4β2, α7 and α9α10 nAChRs, before (grey traces) and after (colour traces) a 3 hour incubation with BAPTA-AM (V_h= −70 mV). *Bottom panels*. Percentage of the initial response remaining after BAPTA incubation. Bars represent mean ± S.E.M., open circles represent individual oocytes (n = 4-10). ****p<0.0001, One-Way ANOVA followed by Dunn's test (α4β2 and α7 nAChRs) or Kruskal-Wallis followed by Holm Sidak's test (α9α10 nAChRs).

Figure 7. Hair cell, but not neuronal, nAChRs show differential current-voltage relationships across species. *Top panels*. Representative I–V curves obtained by the application of voltage ramps (-120 to +50mV, 2 seconds) at the plateau response to 3 µM ACh for α4β2 and α9α10 or by the application of 100 µM ACh at different holding potentials for α7 nAChRs. Values were normalized to the maximal agonist response obtained for each receptor. *Bottom panels*. Ratio of current amplitude at +40 mV relative to -90 mV for each oocyte. Bars represent mean ± S.E.M., open circles represent individual oocytes (n = 5-11). *p<0.05 ****p< 0.0001, One-Way ANOVA followed by Dunn's test (α4β2 and α7 nAChRs) or Kruskal-Wallis followed by Holm Sidak's test (α9α10 nAChRs).

Figure 8. **Hair cell nAChRs show great functional divergence, while functional properties of neuronal nAChRs are conserved.**

PCA was conducted using the experimentally determined biophysical properties (Table S8). Square symbols represent rat nAChRs, circles represent chick nAChRs and triangles represent frog nAChRs, α4β2 nAChRs are shown in shades of green, α7 nAChRs in shades of purple and α9α10 nAChRs in shades of orange. The projected locations of inferred functional states are shown for amniote (stars)

797 and tetrapod (crosses) ancestral receptors and coloured in yellow (α4β2), blue (α7) or pink (α9α10).

798 *Inset*. Biplot of the relative contribution of the five biophysical properties to PC1 and PC2.

799

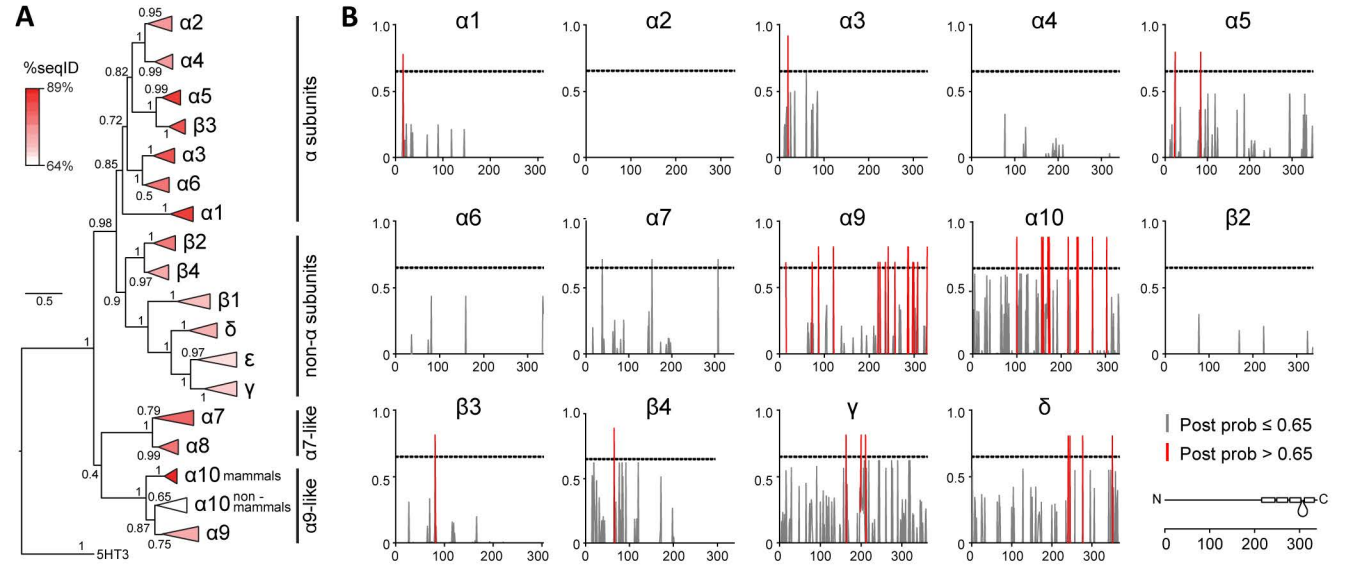
A
%seqID
89%
64%
0.5
α2
α4
α5
β3
α3
α6
α1
β2
β4
β1
δ
ε
γ
α7
α8
α10 mammals
α10 non-mammals
α9
5HT3
α subunits
non-α subunits
α7-like
α9-like
B
α1
α2
α3
α4
α5
α6
α7
α9
α10
β2
β3
β4
γ
δ
Post prob ≤ 0.65
Post prob > 0.65
N
C

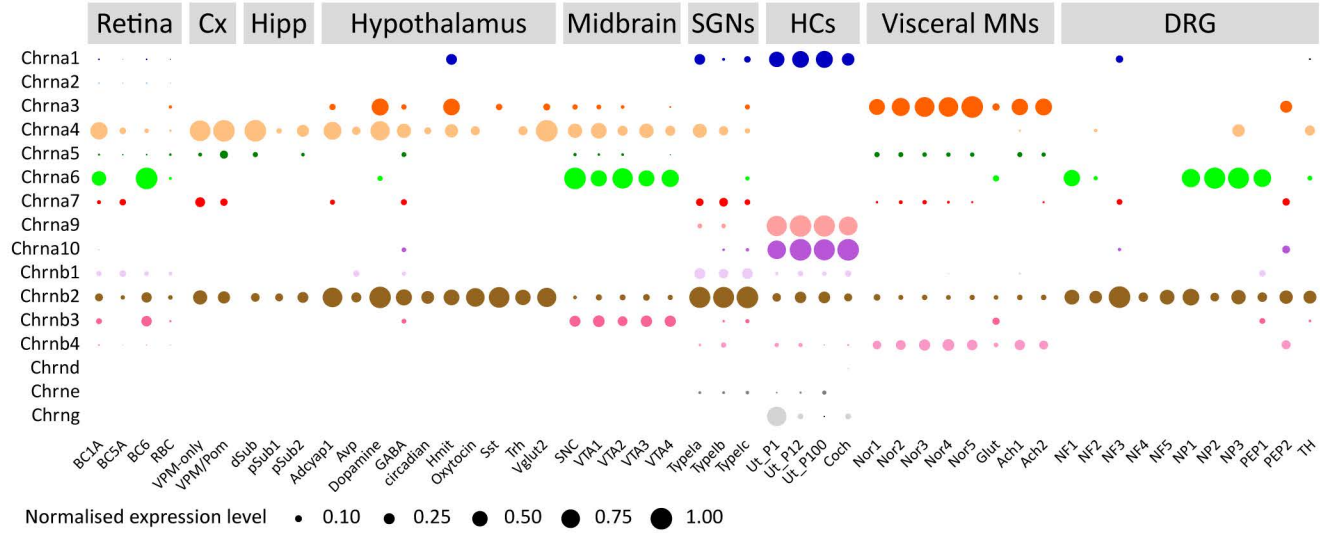
Retina
Cx
Hipp
Hypothalamus
Midbrain
SGNs
HCs
Visceral MNs
DRG
Chrna1
Chrna2
Chrna3
Chrna4
Chrna5
Chrna6
Chrna7
Chrna9
Chrna10
Chrnb1
Chrnb2
Chrnb3
Chrnb4
Chrnd
Chrne
Chrng
BC1A
BC5A
BC6
RBC
VPM-only
VPM/Pom
dSub
pSub1
pSub2
Adcyap1
Avp
Dopamine
GABA
circadian
Hmit
Oxytocin
Sst
Trh
Vglut2
SNC
VTA1
VTA2
VTA3
VTA4
Typela
Typelb
Typelc
Ut_P1
Ut_P12
Ut_P100
Coch
Nor1
Nor2
Nor3
Nor4
Nor5
Glut
Ach1
Ach2
NF1
NF2
NF3
NF4
NF5
NP1
NP2
NP3
PEP1
PEP2
TH
Normalised expression level
0.10
0.25
0.50
0.75
1.00

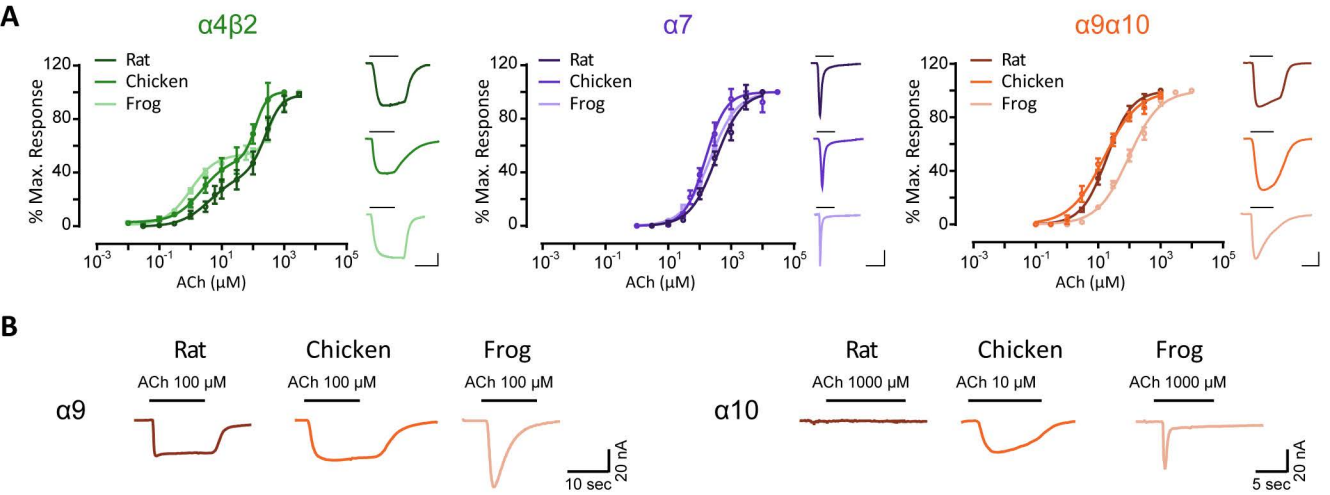
A
α4β2
α7
α9α10
Rat
Chicken
Frog
% Max. Response
ACh (μM)
B
α9
α10
Rat
Chicken
Frog
ACh 100 μM
ACh 1000 μM
ACh 10 μM
10 sec
20 nA
5 sec

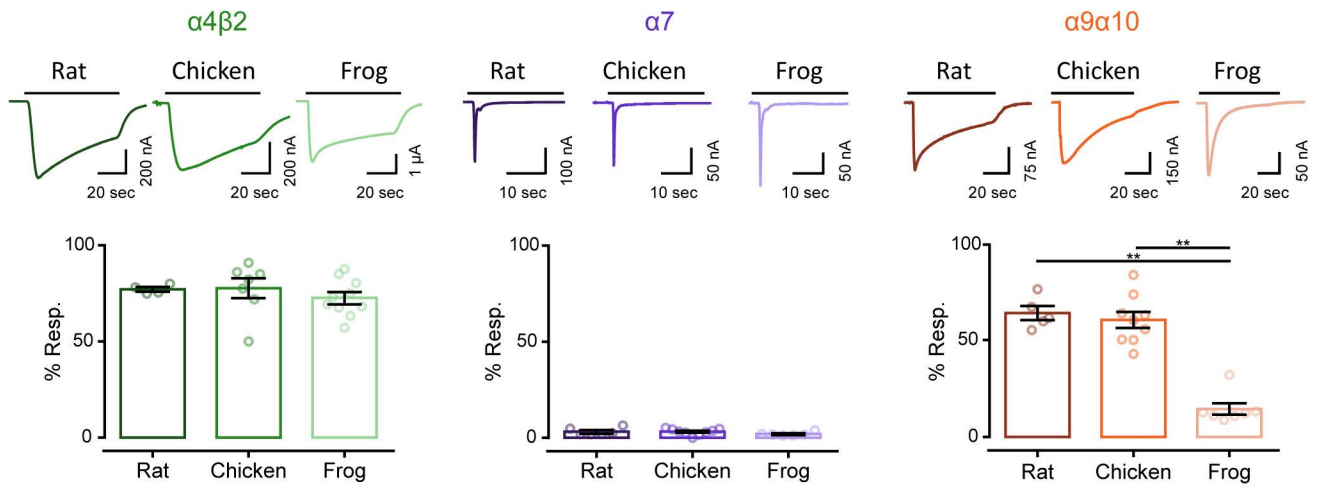
α4β2
α7
α9α10
Rat
Chicken
Frog
200 nA
1 µA
100 nA
50 nA
75 nA
150 nA
20 sec
10 sec
% Resp.
100
50
0
**

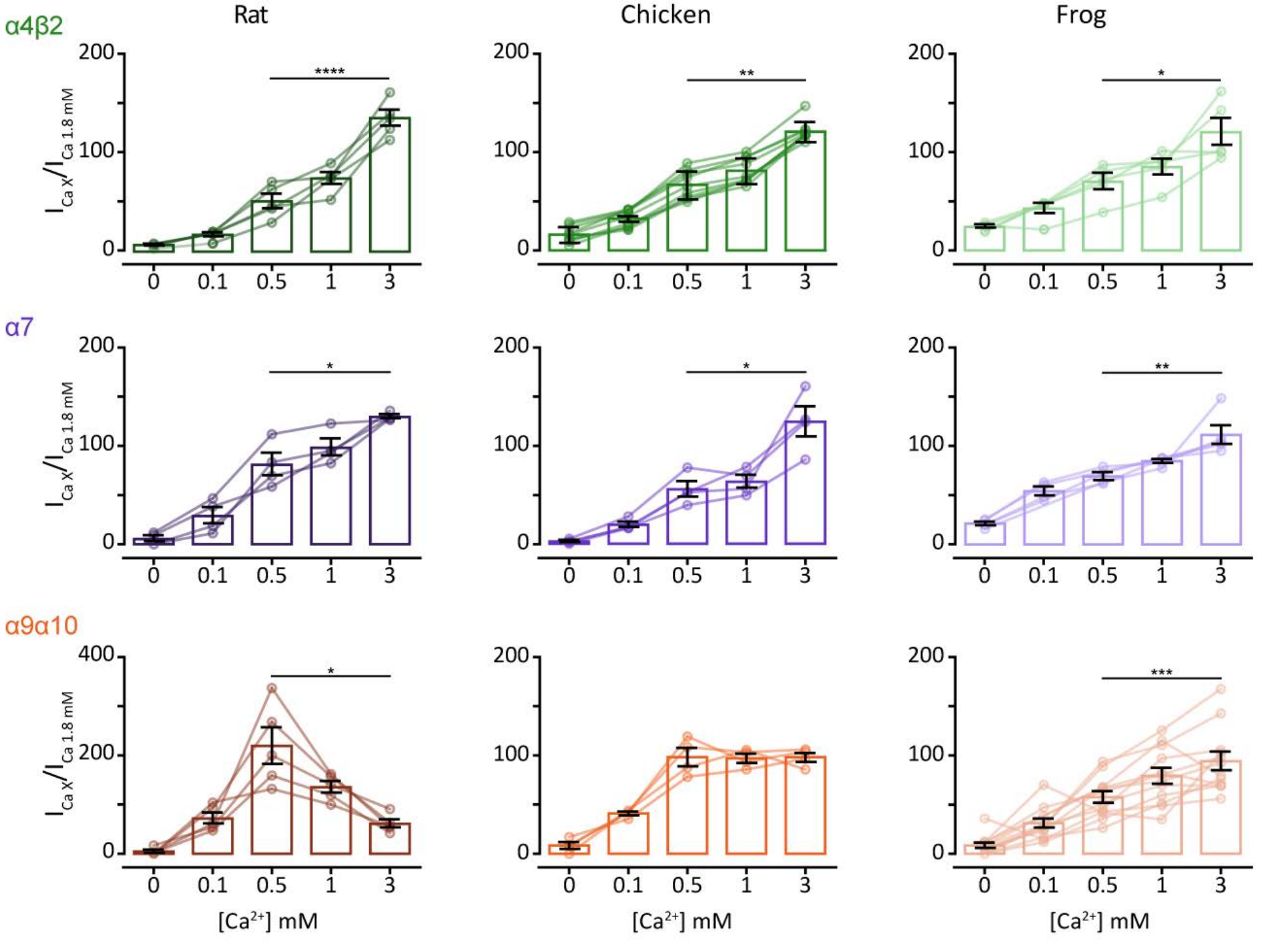
α4β2
α7
α9α10
Rat
Chicken
Frog
$I_{Ca\ X}/I_{Ca\ 1.8\ mM}$
[Ca2+] mM
0
0.1
0.5
1
3
****
**
*
***

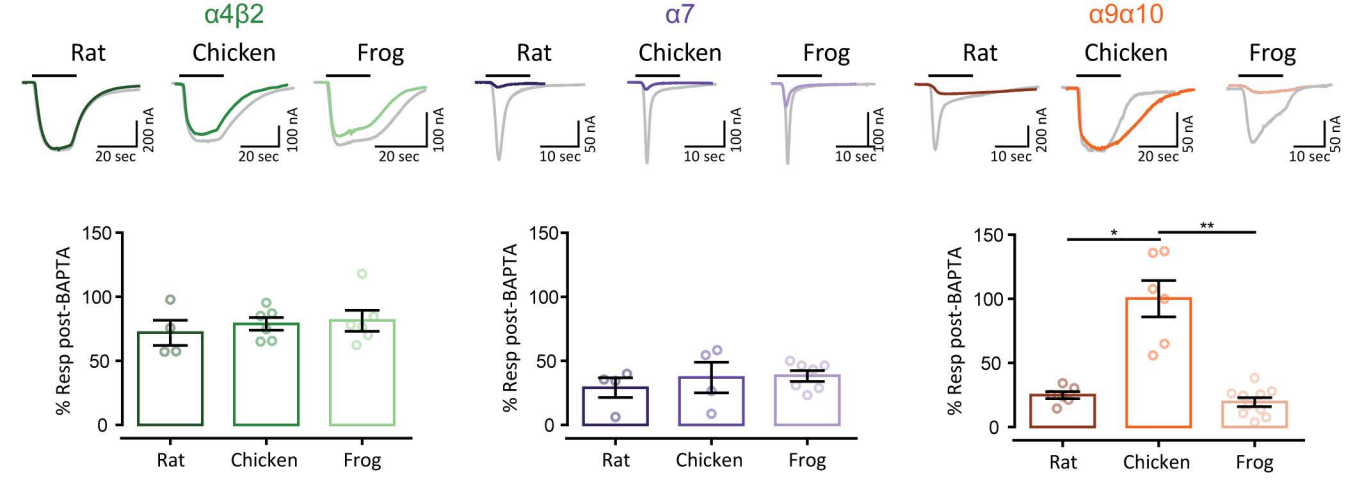
α4β2
α7
α9α10
Rat
Chicken
Frog
Rat
Chicken
Frog
Rat
Chicken
Frog
200 nA
20 sec
100 nA
20 sec
100 nA
20 sec
50 nA
10 sec
100 nA
10 sec
100 nA
10 sec
200 nA
10 sec
50 nA
20 sec
50 nA
10 sec
% Resp post-BAPTA
150
100
50
0
Rat
Chicken
Frog
% Resp post-BAPTA
150
100
50
0
Rat
Chicken
Frog
% Resp post-BAPTA
150
100
50
0
*
**
Rat
Chicken
Frog

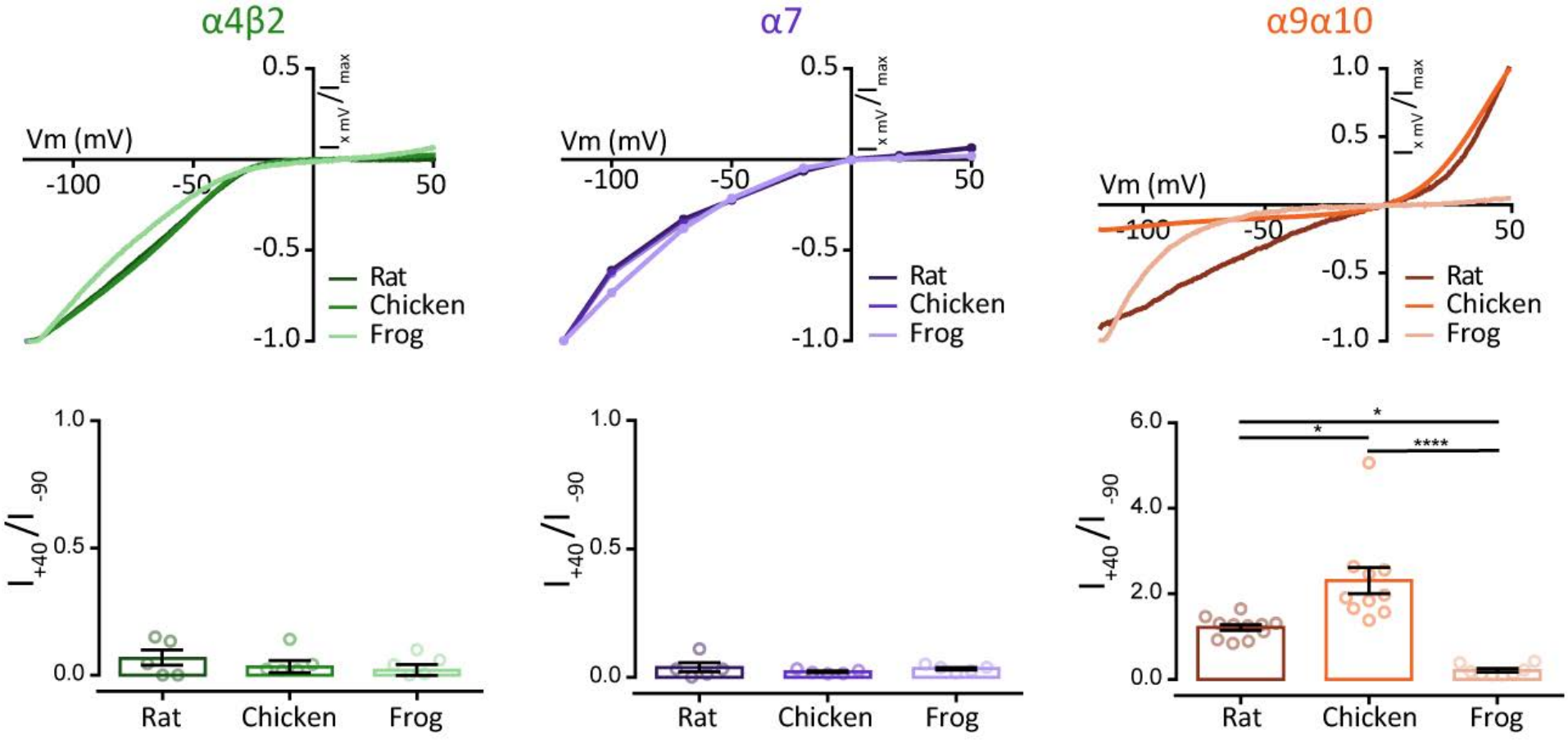
α4β2
α7
α9α10
Vm (mV)
-100
-50
50
0.5
-0.5
-1.0
1.0
$I_{x\,mV}/I_{max}$
Rat
Chicken
Frog
I_{+40}/I_{-90}
0.0
0.5
1.0
2.0
4.0
6.0
*
****

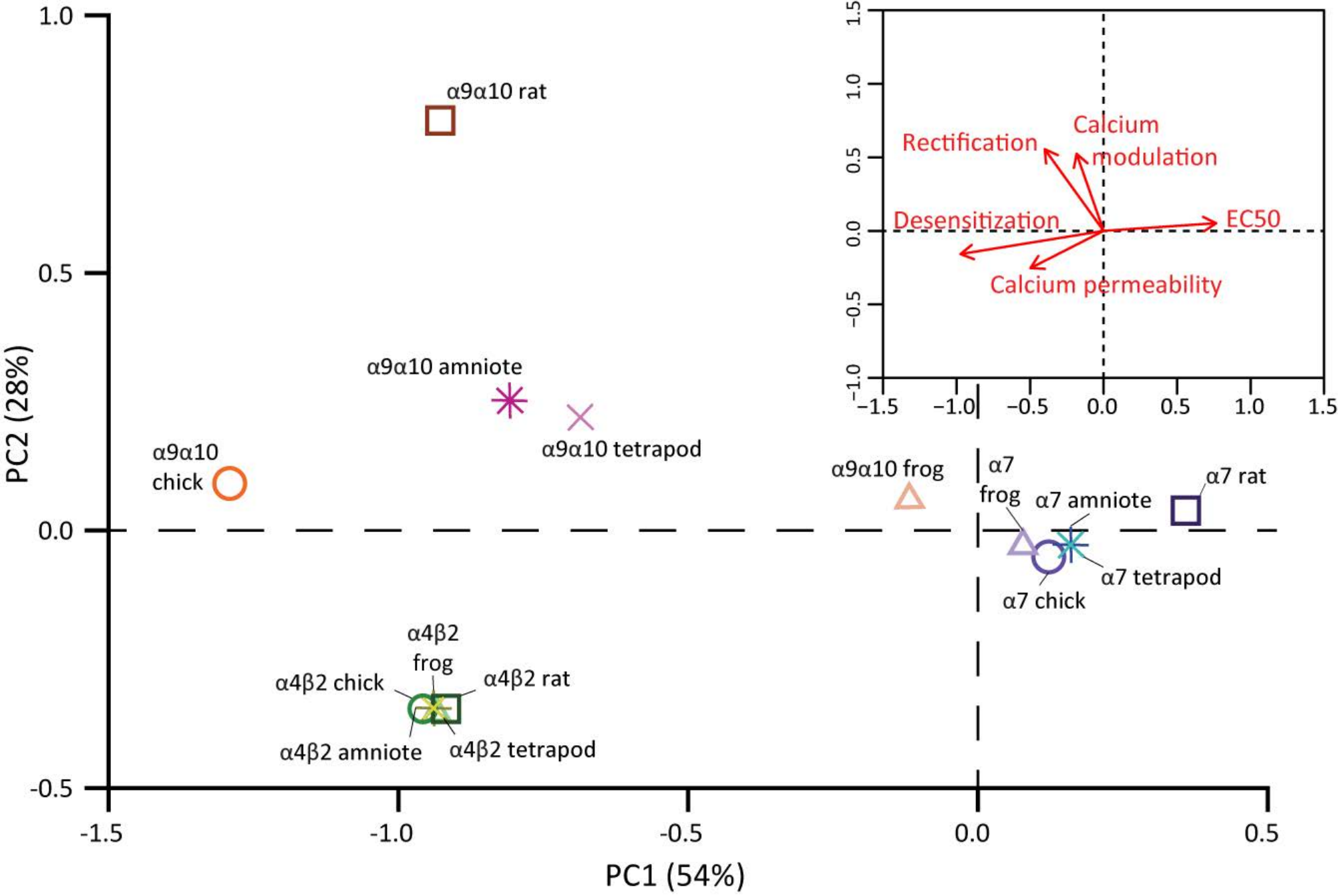
α9α10 rat
α9α10 amniote
α9α10 tetrapod
α9α10
chick
α9α10 frog
α7
frog
α7 amniote
α7 rat
α7 tetrapod
α7 chick
α4β2
frog
α4β2 chick
α4β2 rat
α4β2 amniote
α4β2 tetrapod
Rectification
Calcium
modulation
Desensitization
EC50
Calcium permeability
PC1 (54%)
PC2 (28%)

Supplementary Information for

Distinct evolutionary trajectories of neuronal and hair cell nicotinic acetylcholine receptors

Irina Marcovich[1], Marcelo J. Moglie[1], Agustín E. Carpaneto Freixas[1], Anabella P. Trigila[1], Lucia F. Franchini[1], Paola V. Plazas[2], Marcela Lipovsek*[1,3] and Ana Belén Elgoyhen*[1,2]

[1] Instituto de Investigaciones en Ingeniería Genética y Biología Molecular "Dr. Héctor N. Torres" (INGEBI), Consejo Nacional de Investigaciones Científicas y Técnicas (CONICET), Buenos Aires, Argentina.

[2] Instituto de Farmacología, Facultad de Medicina, Universidad de Buenos Aires, Buenos Aires, Argentina.

[3] Centre for Developmental Neurobiology, King's College London, Institute of Psychiatry, Psychology and Neuroscience, Guy's Campus, London SE1 1UL.

* These authors contributed equally.

Correspondence should be addressed to Marcela Lipovsek (marcela.lipovsek@kcl.ac.uk)

This PDF file includes:

Supplementary text: supplementary methods

Figures S1 to S9

Tables S1 to S11

Legends for Datasets S1 to S5

SI References

Other supplementary materials for this manuscript include the following:

Datasets S1 to S5

Supplementary methods

All experimental protocols were carried out in accordance with the guides for the care and use of laboratory animals of the National Institutes of Health and the Institutional Animal Care and Use Committee of the Instituto de Investigaciones en Ingeniería Genética y Biología Molecular, "Dr. Héctor N. Torres".

Phylogenetic analysis of vertebrate nAChRs subunits

All sequences were downloaded from GenBank (www.ncbi.nlm.nih.gov/genbank), UCSC (http://genome.ucsc.edu/) and Ensembl (www.ensembl.org) databases. The signal peptides of all sequences were excluded from the analysis since they are not present in the mature functional protein. Accession numbers are listed in Table S1. All sequences were visually inspected, and missing and/or incorrect exons were obtained from the NCBI Genome Project traces database (http://blast.ncbi.nlm.nih.gov/Blast.cgi). Sequence alignment was performed using *Clustal*W on the MEGA7 software (www.megasoftware.net; (1)), with the following parameters: for pairwise alignments, gap opening penalty: 10, gap extension penalty: 0.1; for multiple alignments, gap opening penalty: 10, gap extension penalty: 0.2. Protein weight matrix: Gonnet. Residue specific and hydrophilic penalties: ON. Gap separation distance: 4. End gap separation: OFF and no negative matrix was used. The delay divergent cutoff was 30%. The full alignment for the nicotinic subunits from representative vertebrate species is available in Supplementary File 1 in fasta format.

The phylogenetic tree of all nAChR subunits was built using the MEGA7 software. Positions containing alignment gaps and missing data were eliminated only in pairwise sequence comparisons. The final dataset contained a total of 773 positions. The evolutionary distances (i.e., number of amino acid substitutions per site) were computed using the JTT matrix-based method (2). The neighbour-joining algorithm (3) was used to generate the initial tree and branch support was obtained by bootstrap test (1000 replicates) (4). The evolutionary history was inferred using the minimum evolution method (5). A first tree was generated with variation rate among sites modelled by a gamma distribution (Figure S1) and a second tree assuming uniform variation rates among sites (Figure S2). Overall, tree topology was similar between both methods.

Average percentage sequence identity was calculated for each subunit using the percentage of sequence identity between each pair of sequences (Supplementary File 2) from the same category for all sequences and for within or between mammalian and/or sauropsid sequences. For α10 subunits, the average percentage of sequence identity was also calculated for the non-mammalian paraphyletic group. Values obtained are summarised in Table S2.

The cumulative distribution of percentage sequence identity between pairs of sequences from all amniotes and within or between mammalian and/or sauropsid species was plotted for each subunit (Fig. S3).

Functional divergence analysis

The DIVERGE 3.0 software was used to statistically test for functional diversification of nAChR subunits between the mammalian and sauropsid clades. DIVERGE predicts amino acid sites that may be involved in between-clade functional divergence against the background of neutral evolution (6). In particular, it estimates the type II functional divergence coefficient (θ_{II}) that indicates site-specific evolutionary shifts in aminoacid biochemical state between clades and then uses a Bayesian approach to compute the posterior probability that each individual site contributes to the clade-specific functional diversification. Type II sites represent aminoacids that are highly conserved in each clade, but in a biochemically different state (i.e., positively charged in clade 1 and negatively charged in clade 2).

Multiple alignments of protein sequences for each individual subunit were generated using the MEGA7 software as described above. The highly variable amino-terminal signal peptides and intracellular domains were excluded from the analysis. Phylogenetic trees, with a topology corresponding to the species tree, were constructed for each nicotinic subunit by Maximum Likelihood and the JTT matrix-based method (2). The rates among sites were modelled as a gamma distribution. All positions with less than 95% site coverage were eliminated. α8, β1 and ε nAChR subunits were not included in the analysis due to lack of mammalian and/or sauropsid sequences to perform suitable comparisons.

Multiple alignments of protein sequences and their corresponding phylogenetic trees (Supplementary File 3) were used as input data for DIVERGE 3.0 type II functional divergence analysis (7), with default parameters. θ_{II} and site-specific posterior probabilities were calculated for each subunit. A θ_{II} value significantly greater than 0 ($P < 0.05$) indicates that residues conserved within each group have undergone radical changes in amino acid identity between groups (6). z-scores were used to test the significant difference of θ_{II} coefficients against the null hypothesis ($\theta_{II} = 0$) that implies no sites are present in the protein that reflect between-clade functional divergence (Table S3). Site-specific posterior probabilities were computed for all sites along each subunit (Supplementary File 3). Sites with posterior probabilities greater than 0.65 for each subunit are highlighted in Figure 1B.

Analysis of nAChR subunit expression in single-cell RNAseq (scRNAseq) datasets

Processed gene expression data tables were obtained from 10 scRNAseq studies that evaluated gene expression in retina (8) inner ear sensory epithelium (9, 10) and spiral ganglion (11), ventral midbrain (12), hippocampus (13), cortex (14), hypothalamus (15), visceral motor neurons (16) and dorsal root ganglia (17). Accession numbers, cell types inferred and number of cells analysed are summarised in Table S4. For all datasets, we used the published gene expression quantification and cell type labels. Each dataset was analysed separately. For the retina dataset we used the Smart-Seq2 sequencing data from Vsx2-GFP positive cells (8). For the gene expression quantification we only analysed four cell types that had a minimum number of cells in the dataset that allowed reliable fitting to the error models: BC1A, BC5A, BC6 and RBC. From the layer VI somatosensory cortex dataset (13) we used a subset of the expression matrix that corresponds to day 0 (i.e. control, undisturbed neurons) of their experimental manipulation. For the hypothalamic neurons dataset (15) we used a subset that contained only neurons from untreated (control) mice and only quantified gene expression on the 10 broad cell types identified. From the ventral midbrain dopaminergic neurons dataset (12) we used a subset comprising DAT1-Cre/tdTomato positive neurons from P28 mice. For the SGNs dataset we used a subset comprising Type I neurons from wild type mice (11). For the utricle hair cell datasets we used the normalised expression data of (10). For the cochlear hair cell data we used the normalised expression data from (9) and continued our analysis with only the 10 cochlear hair cells identified. For the visceral motor neurons dataset (16) we excluded the neurons that were "unclassified" from further analysis. For the dorsal root ganglia dataset (17) we used a subset containing only successfully classified neurons that were collected at room temperature. Inspection of all datasets for batch effects was performed using the *scater* package (version 1.10.1) (18). Single cell expression of nAChR subunits was initially evaluated on violin plots (Fig. S4). All data analysis was implemented in R (version 3.5.1) and Bioconductor (version 3.8) (http://www.bioconductor.org/), running on RStudio (version 1.1.456) (http://www.rstudio.com/).

The publicly available expression matrices for a number of the datasets contained raw counts (retina, hippocampus, hypothalamus, midbrain, visceral motor neurons). For each of these dataset individually, we performed a normalisation step using the *scran* package (version 1.10.2) (19) that computes pool-based size factors that are subsequently deconvolved to obtain cell-based size factors.

The normalised expression matrices and cell type information were used as input to quantify cell-type specific gene expression. Analysis was performed using the *scde* package (version 1.99.1) (20). We modelled the gene expression measurements from each individual cell as a weighted mixture of negative binomial and low-magnitude Poisson distributions. The former accounts for the correlated component in which a transcript is detected and quantified, while the latter accounts for drop-out

events in which a transcript fails to amplify when present. The weighting of the two distributions is determined by the level of gene expression in the cell population (20). We then used these error models to estimate the likelihood (joint posterior probability) of a gene being expressed at any given average level in a given cell type (20). Probability distributions for all nAChR subunit genes detected in all the cell types analysed are shown in Fig S5. This whole transcriptome analysis provides accurate estimations of gene expression levels, thus allowing for the comparison of individual genes within a given cell type (i.e. the complement of nAChR subunits) or the analysis of expression level differences between cell types (i.e. change in expression level of nAChR subunits between neuronal subtypes). Inferred mean expression values are summarised in Table S5. We combined the information about the complement of nAChR subunits for each cell type with a comprehensive catalogue of experimentally validated subunit combinations (Table S6 and references therein). We identified the subunit combinations that were present, in each cell type, within a 10-fold, 10 to 100-fold or 100 to 1000 fold range of expression level or absent all together. Admittedly, this analysis approach overlooks the complexities of post-translational modifications, receptor assembly, role of chaperone proteins and transport to the plasma membrane. However, it provides conservative estimates of the maximum potential of combinatorial assembly of subunits and thus a maximum for the repertoire of nAChR assemblies that could be present at the cell membrane.

Expression of recombinant receptors in *Xenopus laevis* oocytes and electrophysiological recordings

Rat and chick α9 and α10 cDNAs subcloned into pSGEM, a modified pGEMHE vector suitable for *Xenopus laevis* oocyte expression studies, were described previously (21-23). Rat α4, β2 and α7 subunit cDNAs subcloned into pBS SK(−) (Agilent Technologies, Santa Clara, CA) were kindly provided by Dr. Jim Boulter (University of California, Los Angeles, CA). Chicken α4 and β2 subunit cDNAs subcloned into pCI (Promega, Madison, WI) were kindly provided by Dr. Isabel Bermudez-Díaz (Oxford Brookes University, Oxford, UK). Chicken α7 subunit cDNA cloned into pMXT was kindly provided by Dr. Jon Lindstrom (University of Pennsylvania) and was then subcloned into pSGEM between HindIII and SalI sites. Frog α4, β2, α7, α9 and α10 subunits were cloned from whole brain *Xenopus tropicalis* cDNA. Total RNA was prepared from whole brains using the RNAqueous – Micro kit AM1931 (Ambion, Thermo Fisher Scientific, Boston, MA). First strand cDNA synthesis was performed using an oligodT and the ProtoScript Taq RT-PCR kit (New England Biolabs, Ipswich, MA). Second strand synthesis was performed with the NEBNext mRNA Second Strand Synthesis Module kit – E6111S (New England Biolabs, Ipswich, MA). Full length cDNAs for each subunit were PCR amplified (MultiGene 60 OptiMaxTM Thermal Cycler - Labnet International Inc. Edison, NJ) using specific primers (Table S7). PCR products were sequenced and subcloned into pSGEM between EcoRI and XhoI sites for α9, α7 and β2 nAChRs subunits, between HindIII and XhoI sites for the α10 subunit

and between EcoRI and HindIII sites for the α4 subunit. All expression plasmids are readily available upon request.

Capped cRNAs were *in vitro* transcribed from linearized plasmid DNA templates using the RiboMAX^{TM} Large Scale RNA Production System-T7 (Promega, Madison, WI). The maintenance of *Xenopus laevis*, as well as the preparation and cRNA injection of stage V and VI oocytes, has been described in detail elsewhere (Katz et al., 2000). Briefly, oocytes were injected with 50 nl of RNase-free water containing 0.01–1.0 ng of cRNAs (at a 1 : 1 molar ratio for α9α10 and α4β2 receptors) and maintained in Barth's solution (in mM): NaCl 88, $Ca(NO_3)_2$ 0.33, $CaCl_2$ 0.41, KCl 1, $MgSO_4$ 0.82, $NaHCO_3$ 2.4, HEPES 10, at 18ºC.

Electrophysiological recordings were performed 2 – 6 days after cRNA injection under two-electrode voltage clamp with an Oocyte Clamp OC-725B or C amplifier (Warner Instruments Corp., Hamden, CT). Recordings were filtered at a corner frequency of 10 Hz using a 900BT Tunable Active Filter (Frequency Devices Inc., Ottawa, IL). Data acquisition was performed using a Patch Panel PP-50 LAB/1 interface (Warner Instruments Corp., Hamden, CT) at a rate of 10 points per second. Both voltage and current electrodes were filled with 3M KCl and had resistances of ~1MΩ. Data were analysed using Clampfit from the pClamp 6.1 software (Molecular Devices, Sunnyvale, CA). During electrophysiological recordings, oocytes were continuously superfused (10 ml min^{-1}) with normal frog saline composed of (in mM): 115 NaCl, 2.5 KCl, 1.8 $CaCl_2$ and 10 HEPES buffer, pH 7.2. In order to minimize the activation of the oocyte's native Ca^{2+}-sensitive chloride current (ICl_{Ca}) by inward Ca^{2+} current through the nAChRs, all experiments, unless otherwise stated, were carried out in oocytes incubated with the membrane permeant Ca^{2+} chelator 1,2-bis (2-aminophenoxy)ethane-N,N,N',N'-tetraacetic acid-acetoxymethyl ester (BAPTA-AM; 100 μM) for 3 h prior to electrophysiological recordings. This treatment was previously shown to effectively chelate intracellular Ca^{2+} ions and, therefore, to impair the activation of the ICl_{Ca} (24). All recordings were performed at -70 mV holding potential, unless otherwise stated.

Biophysical properties of nAChRs

Concentration-response curves were obtained by measuring responses to increasing concentrations of ACh. Current amplitudes were normalized to the maximal agonist response in each oocyte. The mean and S.E.M. values of the responses are represented. Agonist concentration-response curves were iteratively fitted, using Prism 6 software (GraphPad Software Inc., La Jolla, CA), with the equation: I/Imax = AnH / (AnH + EC_{50}nH), where I is the peak inward current evoked by the agonist at concentration AnH; Imax is current evoked by the concentration of agonist eliciting a maximal

response; EC_{50} is the concentration of agonist inducing half-maximal current response and nH is the Hill coefficient.

Desensitisation of ACh evoked currents was evaluated via prolonged agonist applications. The percentage of current remaining 5 seconds (for α7 nAChRs) or 20 seconds (for α4β2 and α9α10 nAChRs) after the peak of the response was determined for each oocyte.

The effects of extracellular Ca^{2+} on the ionic currents through nAChRs were studied by measuring the amplitudes of the responses to a near-EC_{50} concentration of ACh (10 μM for all α4β2 and amniote α9α10 nAChRs, and 100 μM for all α7 and frog α9α10 nAChRs) on extracellular Ca^{2+} ranging from nominally 0 to 3 mM at a holding potential of -90 mV (25). These experiments were carried out in oocytes injected with 7.5 ng of an oligonucleotide (5'-GCTTTAGTAATTCCCATCCTGCCATGTTTC-3') antisense to connexinC38 mRNA (26, 27) to minimise the activation of the oocyte's nonselective inward current through a hemigap junction channel that results from the reduction of external divalent cation concentration. Current amplitudes at each Ca^{2+} concentration were normalized to that obtained in the same oocyte at a 1.8 mM Ca^{2+}.

I–V relationships were obtained by applying 2 seconds voltage ramps from -120 to +50 mV from a holding potential of -70 mV, at the plateau response to 3 μM ACh. Leakage correction was performed by digital subtraction of the I–V curve obtained by the same voltage ramp protocol prior to the application of ACh. Generation of voltage protocols and data acquisition were performed using a Patch Panel PP-50 LAB/1 interface (Warner Instruments Corp., Hamden, CT) at a rate of 10 points per second and the pClamp 7.0 software (Axon Instruments Corp., Union City, CA). Current values were normalized to the maximum amplitude value obtained for each oocyte. The fast desensitising α7 receptors had negligible plateau currents. For these receptors, responses to 100 μM ACh were obtained at different holding potentials and normalised to the amplitude response at -120 mV in the same oocyte.

Table S8 summarises the biophysical properties and statistical comparisons from rat, chicken and frog α4β2, α7 and α9α10 receptors.

Statistical analysis

Shapiro-Wilks normality test was conducted using custom routines written in R v3.4.1 (R Development Core Team, 2008), through RStudio software v1.0.153. Statistical significance was determined using either parametric paired *t*-test or One-way ANOVA followed by Holm-Sidak's test, or nonparametric Wilcoxon or Kruskal-Wallis tests followed by Dunn's tests conducted using Prism 6 software (GraphPad Software Inc., La Jolla, CA). A $p< 0.05$ was considered significant.

Reagents

All drugs were obtained from Sigma-Aldrich (Buenos Aires, Argentina). ACh chloride was dissolved in distilled water as 100 mM stocks and stored aliquoted at -20°C. BAPTA-AM was stored at -20°C as aliquots of a 100 mM stock solution in dimethylsulfoxide, thawed and diluted into Barth's solution shortly before incubation of the oocytes. ACh solutions in Ringer's saline were freshly prepared immediately before application.

Principal component analysis of functional properties

Principal Component Analysis was performed on the experimental values obtained for the functional properties of extant nAChRs implementing custom routines written in R v3.4.1 and run in RStudio software v1.0.153. Each of the experimental variables was normalized to the maximum value recorded to allow for equal weighting of the properties (Table S9). The loadings of the empirical variables on the five principal components (PC) generated are shown in Table S10, alongside the proportion of the total variability explained by each component. The loadings of each biophysical property on each principal component are also shown on the vectors biplot (Figure 8 – inset).

Inference of character state of functional properties of ancestral receptors

The pipeline followed to infer the ancestral character state of biophysical properties of nAChRs is schematized on Fig. S7. Briefly, we first reconstructed the ancestral tetrapods and amniote DNA sequences of the α4, α7, α9, α10 and β2 nAChRs subunits (Supplementary File 4). For that purpose, we used the same orthologue sequences that were used to construct the phylogenetic tree of Figure 1, together with a species tree with no branch lengths obtained from Ensembl (https://www.ensembl.org/info/about/speciestree.html). Inferred ancestral DNA sequences for the amniote and tetrapod nodes (Supplementary File 4) were obtained, for all three codon positions, by the maximum likelihood method (28) under the Tamura-Nei model (29), on the MEGA7 software (1). The initial tree corresponds to the provided Species Tree with very strong restriction to branch swap. The rates among sites were treated as a gamma distribution. All positions with less than 95% site coverage were eliminated.

Subsequently, multiple alignments including extant rat, chick and frog and ancestral amniote and tetrapod aminoacid sequences were performed using MEGA7 for each studied nAChR (Supplementary File 5). The sequence identity was used to assign branch length values to α7, α4β2 and α9α10 nAChRs trees, corresponding to 1-SeqID (Table S11). Theoretical concatemeric constructions were built for the heteromeric α9α10 nAChRs considering the descripted prevalent $(\alpha9)_2(\alpha10)_3$ stoichiometry (Plazas et al., 2005). For the α4β2 nAChRs, the high sensitivity $(\alpha4)_2(\beta2)_3$ stoichiometry was used to generate the theoretical concatemeric receptor (Supplementary File 5).

The resulting trees (Fig. S8) were used, together with the biophysical properties experimentally determined for the extant receptors (Table S8) as input data for ancestral character inference. ACh sensitivity (EC_{50} values), desensitization rates (% of remaining *I* 20 sec after ACh peak), Ca^{2+} modulation (*I* elicited by ACh at Ca 0.5 mM/Ca 3 mM), Ca^{2+} permeability (% of remaining *I* after BAPTA treatment) and rectification profile ($I_{+40\ mV}/I_{-90\ mV}$) for the ancestral amniote and tetrapod receptors were inferred using the *ace* function from the *APE* package v5.2 (30) implemented in R v3.4.1 and RStudio v1.0.153. We used the Brownian motion model (31) (Schluter et al., 1997), where characters evolve following a random walk fitted by maximum likelihood (32) for the ancestral character estimations of continuous traits. Reconstructed ancestral states are shown in Fig. S9. Finally, using the loadings of the biophysical properties on PC1 and 2 (Table S10 and Figure 8 – inset), and the normalized *in silico* reconstructed biophysical properties inferred for the ancestral receptors we calculated their position on the bidimensional PCA space (Figure 8).

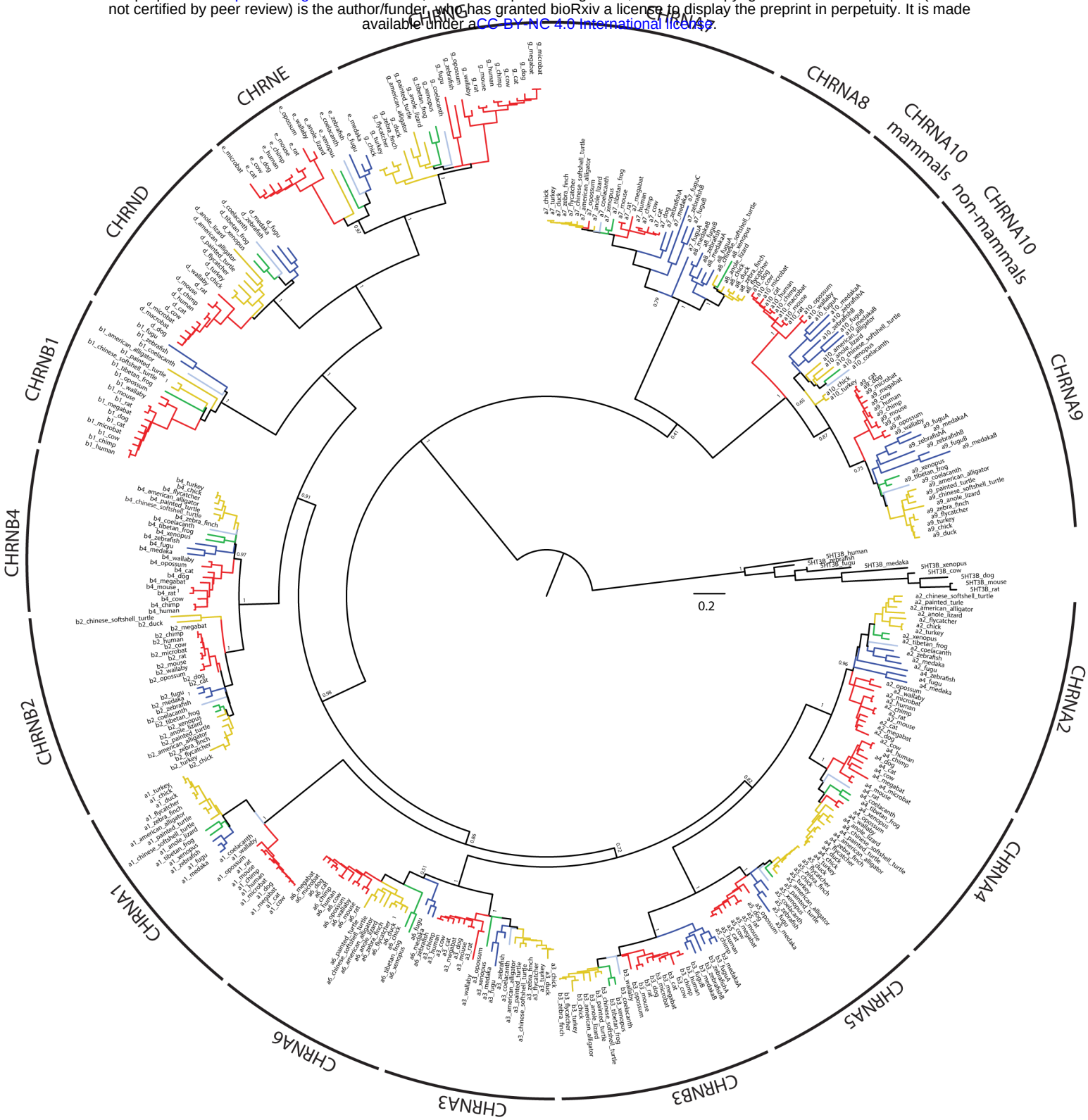

Supplementary Figure 1. Complete minimum evolution phylogenetic tree corresponding to the collapsed tree shown in Figure 1, obtained with variation rates among sites modelled by a gamma distribution. Red branches, mammals; yellow branches, sauropsids; green branches, amphibians; blue branches, fish; light blue branches, coelacanth. The trees were built using minimum evolution method and pairwise deletion for missing sites. The optimal tree with a sum of branch length of 47.32565515 is shown. For clarity, the percentage of replicate trees in which the associated taxa clustered together in the bootstrap test (1,000 replicates) are shown only next to the branches that separate different subunits. The tree is drawn to scale, with branch lengths in the same units as those of the evolutionary distances used to infer the tree.

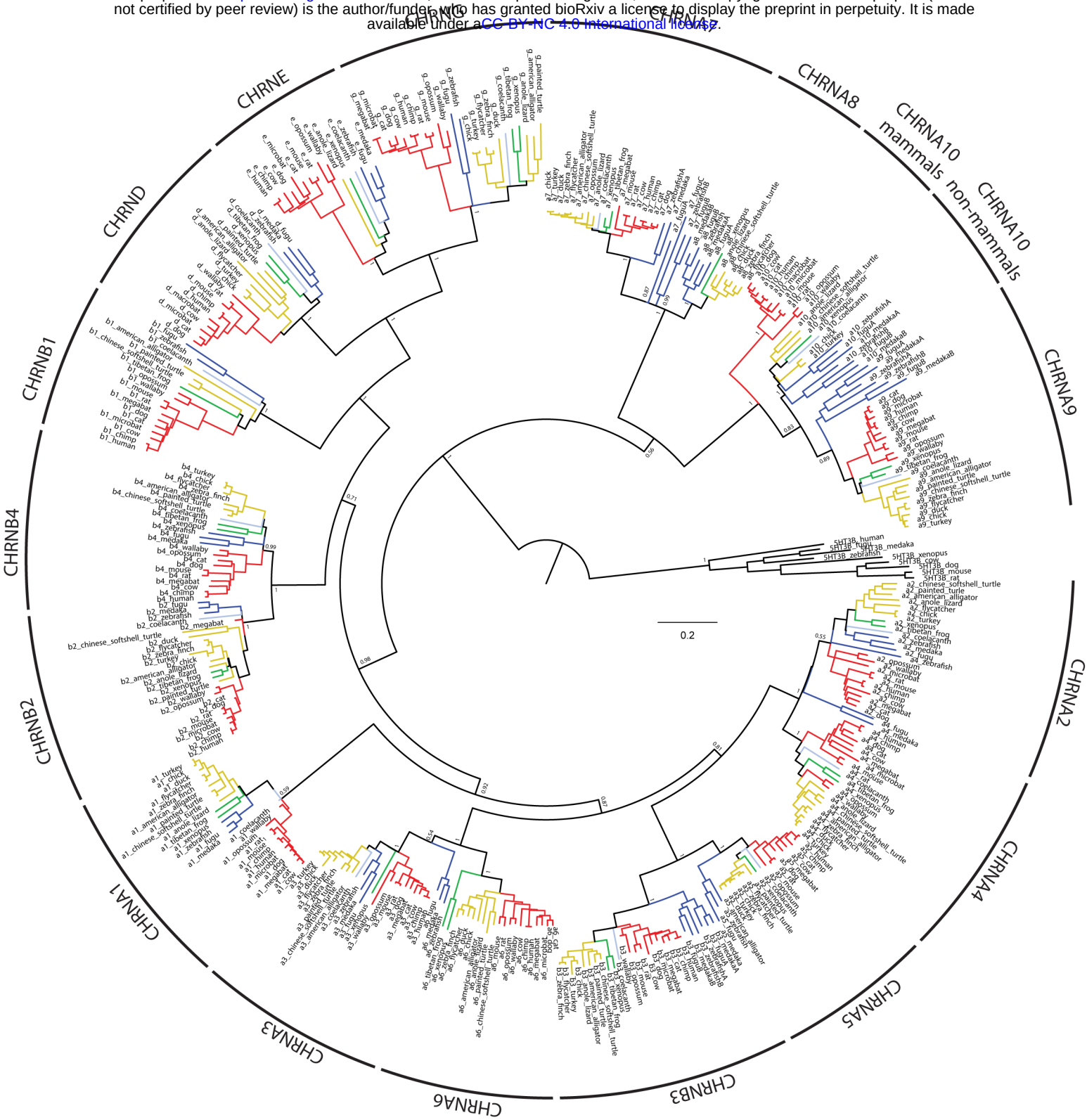

Supplementary Figure 2. Complete minimum evolution phylogenetic tree obtained assuming uniform variation rates among branches. Red branches, mammals; yellow branches, sauropsids; green branches, amphibians; blue branches, fish; light blue branches, coelacanth. The trees were built using minimum evolution method and pairwise deletion for missing sites. The optimal tree with a sum of branch length of 37.49411418 is shown. For clarity, the percentage of replicate trees in which the associated taxa clustered together in the bootstrap test (1,000 replicates) are shown only next to the branches that separate different subunits. The tree is drawn to scale, with branch lengths in the same units as those of the evolutionary distances used to infer the tree.

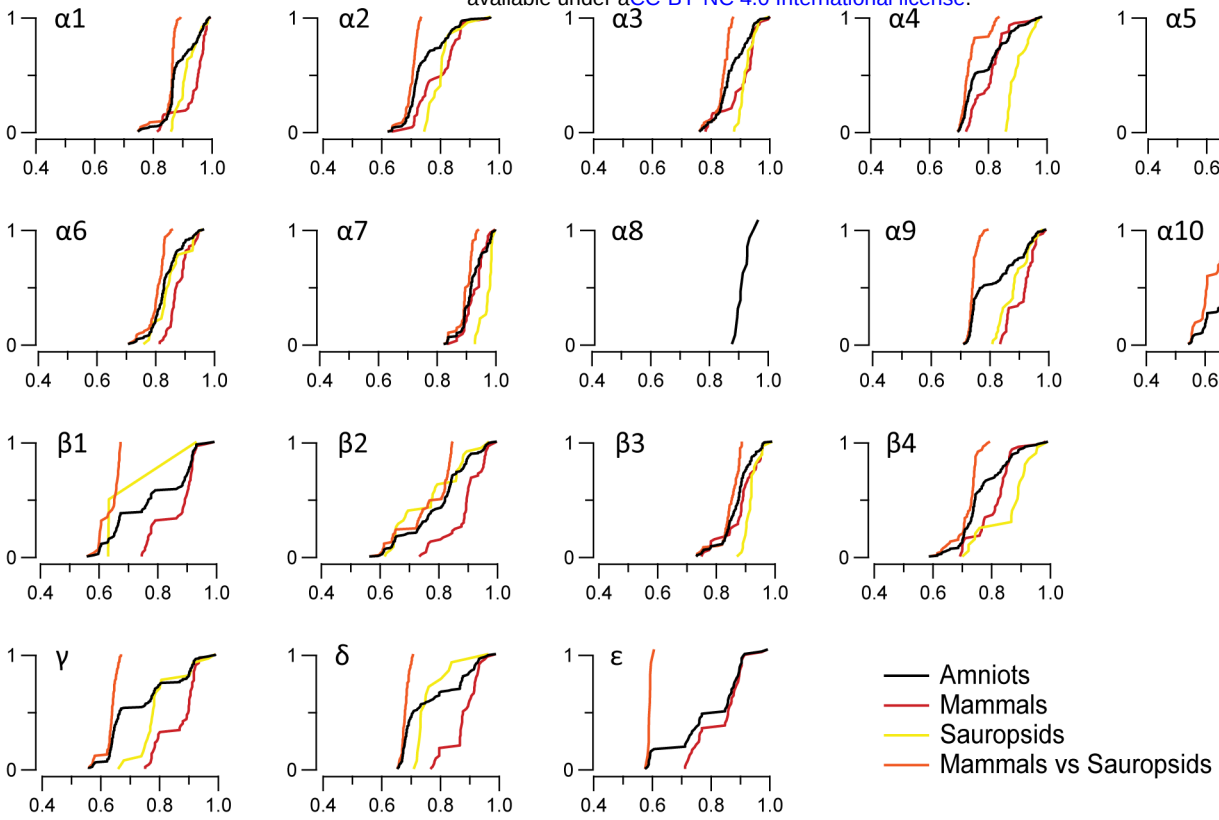

Supplementary Figure 3. Cumulative distributions of sequence identity of individual nAChR subunits. Cumulative distributions were calculated from the sequence identity values obtained for each pair of subunits included in the following groups: only mammalian sequences (red), only sauropsid sequences (yellow), mammalian versus sauropsid sequences (orange) and all mammalian and sauropsid (amniote) sequences (grey).

Supplementary Figure 4. Violin plots showing expression level for all nAChR subunits and acetylcholinesterase (AChE) in the different cell types from the datasets analysed. Expression values are in log2 normalised counts (see methods for details).

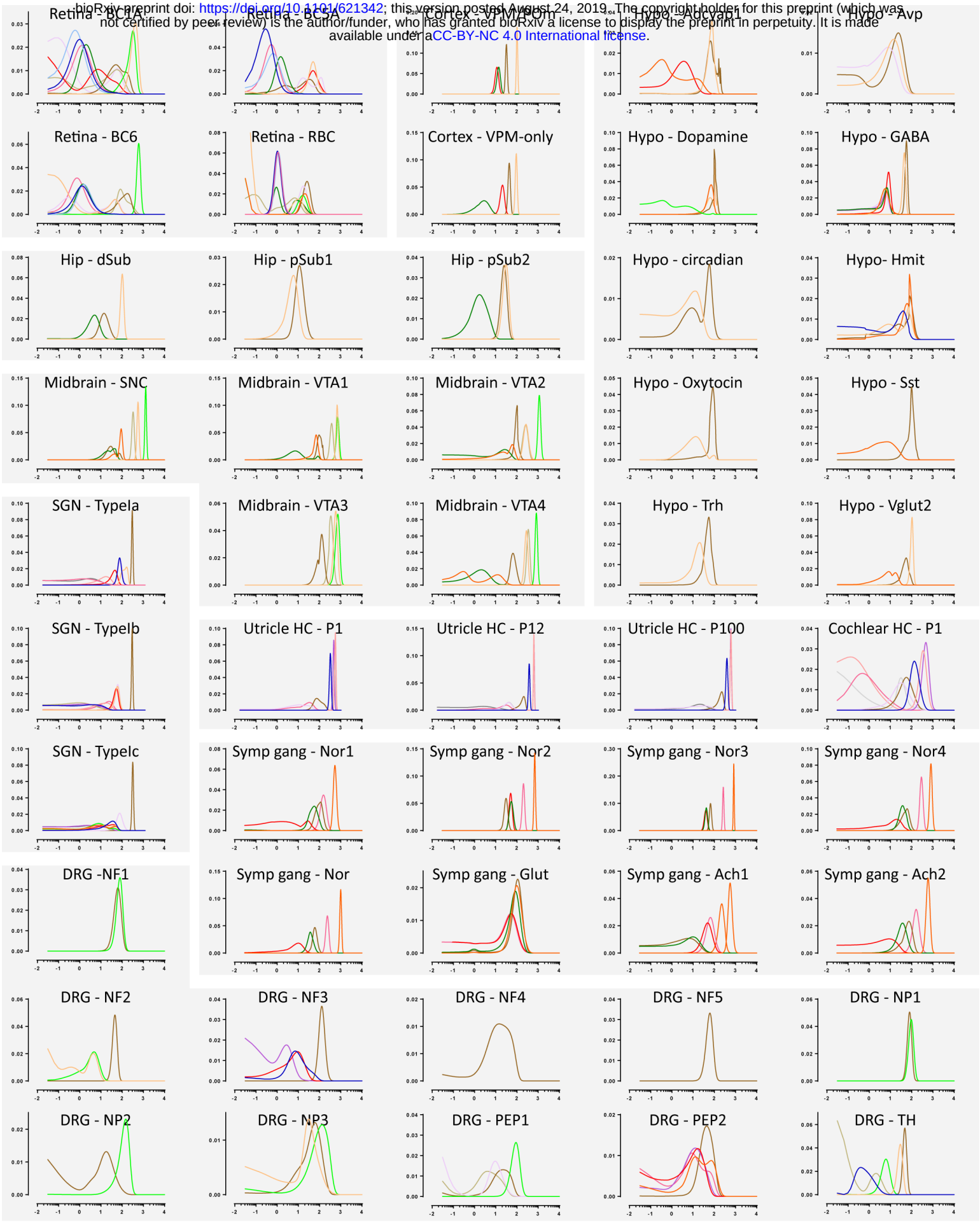

Supplementary Figure 5. Joint posterior probabilities of gene expression levels inferred for the nAChR subunits expressed in the cell types and datasets analysed (see SI Methods for details).

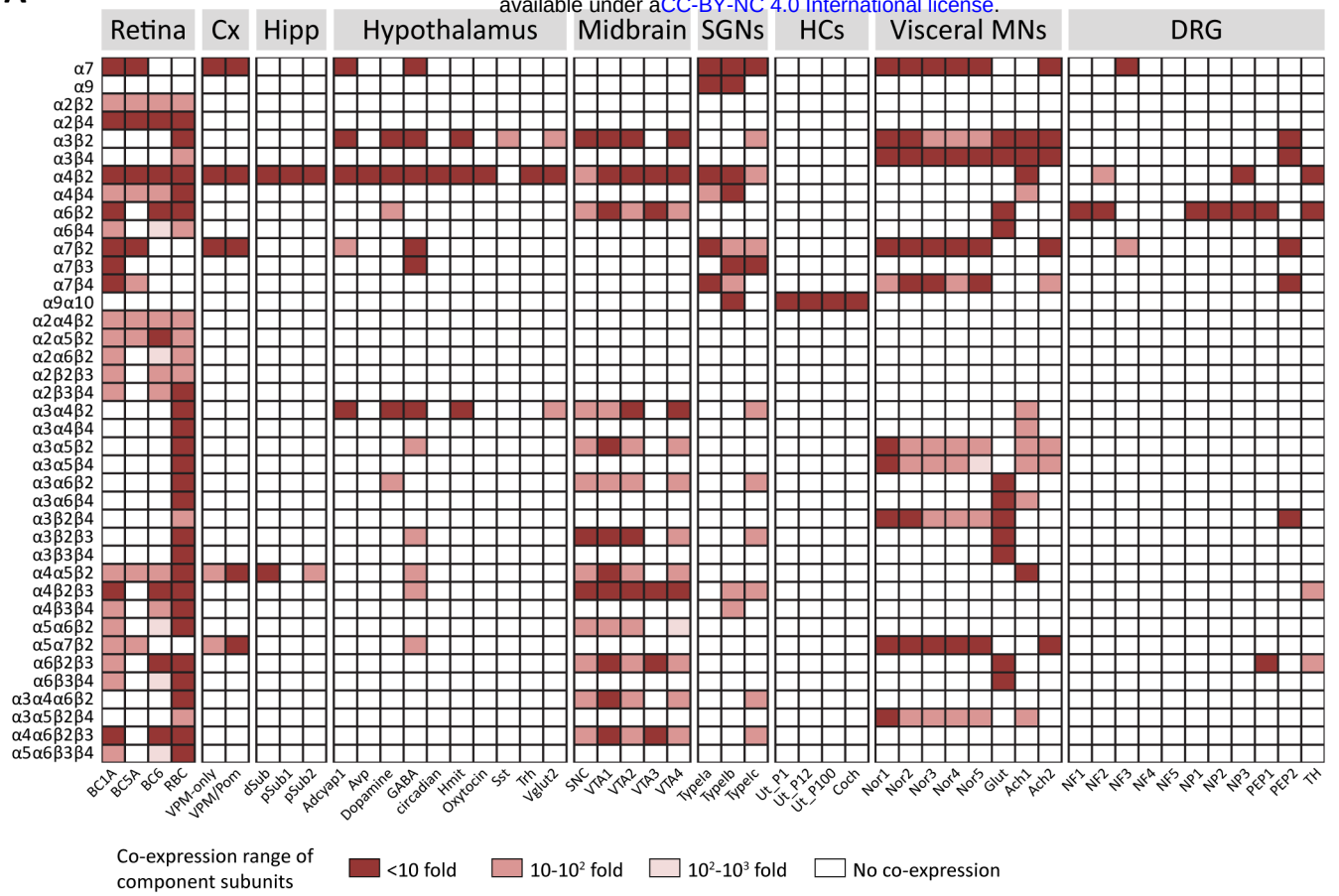

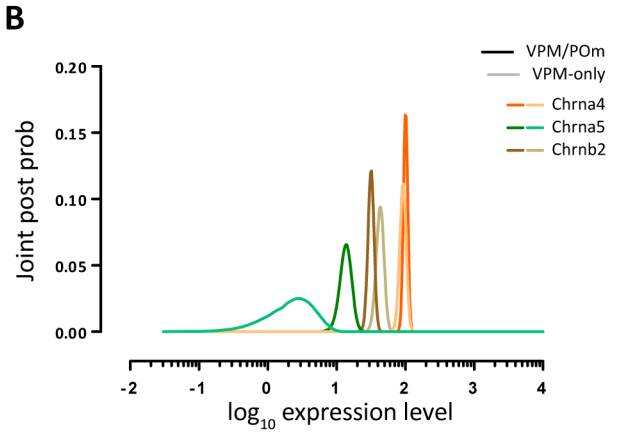

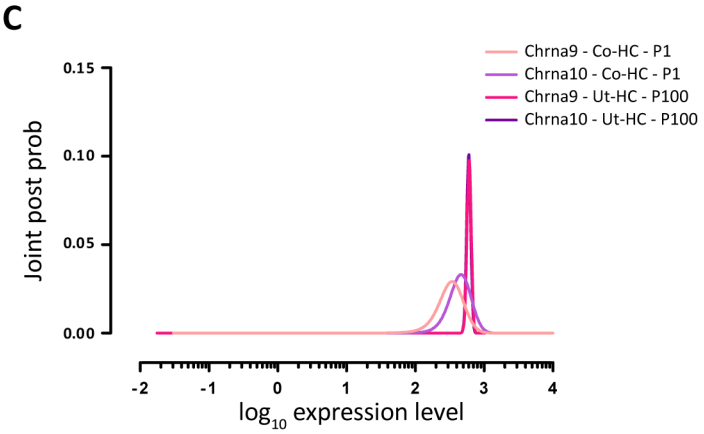

Supplementary Figure 6. A. Co-expression of subunits comprising known nAChR assemblies. Dark red squares, all component subunits are co-expressed within a 10-fold range of expression level. Light red squares, all component subunits are co-expressed within a 100-fold range of expression level. Pink squares, all component subunits are expressed within a 1000-fold range of expression level. White squares, at least one subunit of that receptor assembly in not expressed in that cell type. **B.** Estimated joint posterior probability distributions for expression levels of Chrna4, Chrna5 and Chrnb2 in VPM-only and VPM/POm projecting layer VI neurons. **C.** Estimated joint posterior probability distributions for expression levels of Chrna9 and Chrna10 in inner ear cochlear hair cells (P1) and utricle hair cells (P100).

1. Ancestral DNA sequence reconstruction

2. nAChRs tree generation

3. Ancestral character state inference

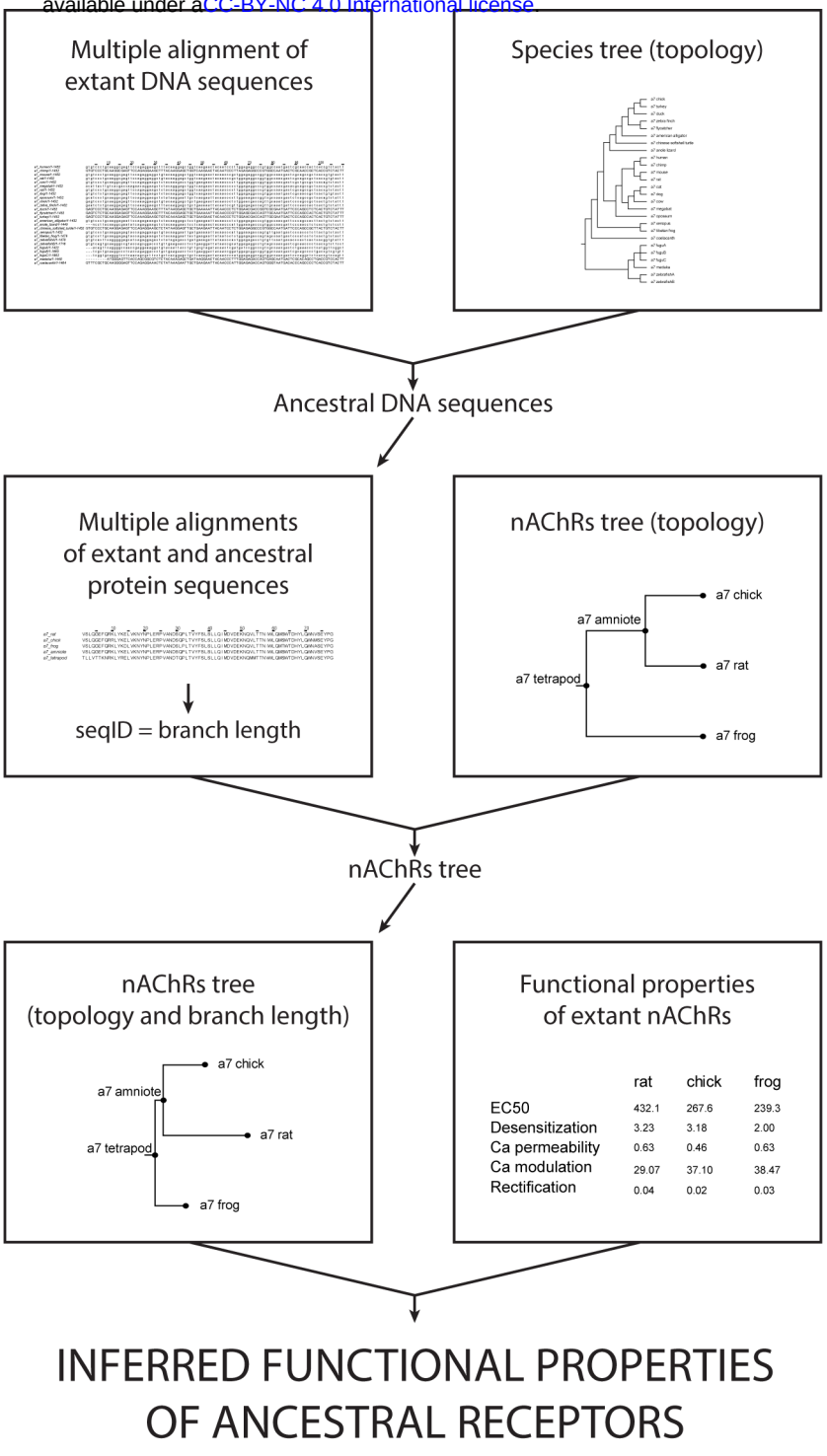

Supplementary Figure 7. Experimental workflow detailing the steps followed for the inference of ancestral character states of the functional properties of tetrapod and amniote ancestral α4β2, α7 and α9α10 receptors.

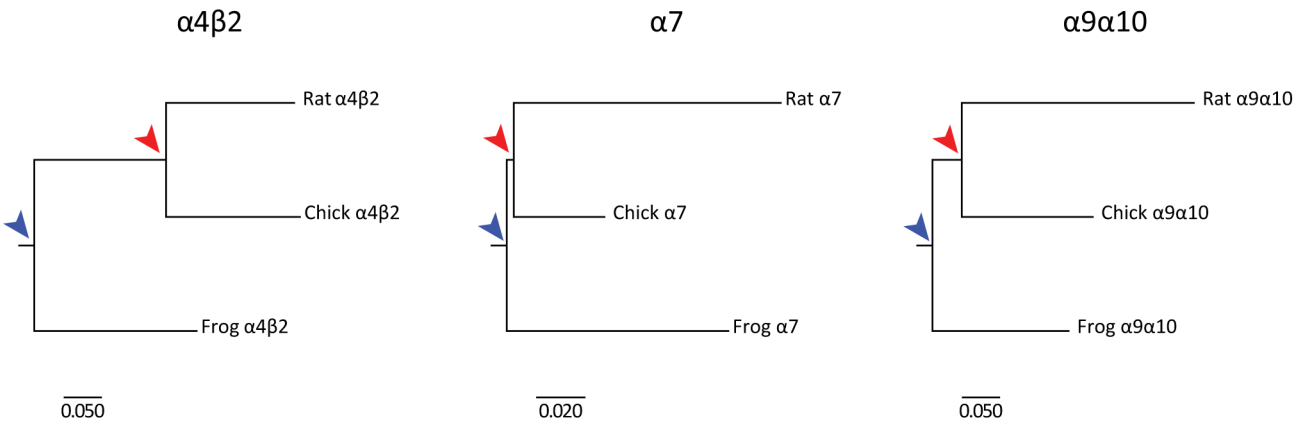

Supplementary Figure 8. nAChRs trees used for the inference of ancestral state states. The tree topology corresponds to the species phylogenetic relationship. The branch lengths correspond to those determined from aminoacid sequence identity analysis between rat-amniote, chick-amniote, amniote-tetrapod and frog-tetrapod pairs of subunits. For the heteromeric α4β2 receptors, branch lengths were calculated assuming a (α4)2(β2)3 assembly. For the heteromeric α9α10 receptors branch lengths were calculated assuming a (α9)2(α10)3 stoichiometry (Plazas et al., 2005). Blue arrows, tetrapod ancestor. Red arrows, amniote ancestor.

	EC_{50} 1	EC_{50} 2	Desensitization	Ca^{2+} modulation	Ca^{2+} permeability	Rectification
α4β2 frog	0.75	143.71	72.70	0.60	81.51	0.02
α4β2 tetrapod	**1.37**	**130.26**	**74.82**	**0.53**	**78.72**	**0.03**
α4β2 chick	1.07	66.00	77.68	0.55	78.75	0.03
α4β2 amniote	**1.86**	**119.34**	**76.54**	**0.48**	**76.46**	**0.04**
α4β2 rat	3.11	159.76	77.13	0.36	72.07	0.07
α7 frog	239.27		2.00	0.63	38.47	0.03
α7 tetrapod	**291.59**		**2.89**	**0.53**	**35.92**	**0.03**
α7 chick	267.56		3.18	0.46	37.10	0.02
α7 amniote	**293.28**		**2.92**	**0.53**	**35.83**	**0.03**
α7 rat	432.10		3.23	0.63	29.07	0.04
α9α10 frog	110.89		14.53	0.63	19.56	0.21
α9α10 tetrapod	**60.27**		**40.55**	**1.38**	**48.80**	**1.14**
α9α10 chick	17.62		60.84	1.00	100.28	2.31
α9α10 amniote	**49.39**		**46.14**	**1.54**	**55.09**	**1.34**
α9α10 rat	19.39		64.46	3.76	24.89	1.21

Supplementary Figure 9. Inferred ancestral character states for amniote and tetrapod α9α10, α4β2 and α7 nAChRs. The biophysical properties of ancestral receptors inferred by maximum likelihood are shown in black. The values in grey correspond to the biophysical properties of extant receptors determined experimentally (Table S7) and used as input for the inference of ancestral character state. The symbols next to each receptor correspond to the symbols in Figure 8.

Table S1. Accession numbers for sequences used in the phylogenetic analysis.

	CHRNA1	CHRNA2	CHRNA3	CHRNA4	CHRNA5	CHRNA6	CHRNA7	CHRNA8	CHRNA9	CHRNA10	CHRNB 1	CHRNB 2	CHRNB 3	CHRNB 4	CHRND	CHRNE	CHRNG	5HT3B
Opossum	ENSMODG00000009414	ENSMODG00000015940	ENSMODG00000011883	ENSMODG00000016860	ENSMODG00000011857	ENSMODG00000010120	ENSMODG00000008920	-	ENSMODG00000020560	ENSMODG00000008246	ENSMODG00000006951	ENSMODG00000017165	ENSMODG00000010082*	ENSMODG00000011891	ENSMODG00000002646*	ENSMODG00000005395	ENSMODG00000002666*	
Wallaby	ENSMEUG00000003627*	ENSMEUG00000004558*	ENSMEUG00000010338*	ENSMEUG00000006728*	-	ENSMEUG00000011281*	ENSMEUG00000009840*	-	ENSMEUG00000010143*	ENSMEUG00000009564*	ENSMEUG00000008924*	ENSMEUG00000003725*	ENSMEUG00000011355*	ENSMEUG00000001043*	ENSMEUG00000011484*	ENSMEUG00000012185*	ENSMEUG00000011510*	
Rat	ENSRNOG00000018286	ENSRNOG00000017424	ENSRNOG00000013829	ENSRNOG00000011202	ENSRNOG00000013610	ENSRNOG00000012283	ENSRNOG00000010853	-	ENSRNOG00000002484	ENSRNOG00000020293	ENSRNOG00000014698	ENSRNOG00000020778	ENSRNOG00000012448	ENSRNOG00000014427	ENSRNOG00000019527	ENSRNOG00000003777	NM_019145.1	
Mouse	ENSMUSG00000027107	ENSMUSG00000022041	ENSMUSG00000032303	ENSMUSG00000027577	ENSMUSG00000035594	ENSMUSG00000031491	ENSMUSG00000030525	-	ENSMUSG00000029205	ENSMUSG00000066279	ENSMUSG00000041189	ENSMUSG00000027950	ENSMUSG00000031492	ENSMUSG00000035200	ENSMUSG00000026251	ENSMUSG00000014609	ENSMUSG00000026253	ENSMUSG00000008590
Cat	ENSFCAG00000014103*	ENSFCAG00000028158	ENSFCAG00000001932	ENSFCAG00000030656	ENSFCAG00000001930	ENSFCAG00000022358	ENSFCAG00000036300	-	ENSFCAG00000035547	ENSFCAG00000023105	ENSFCAG00000009612	ENSFCAG00000022169*	ENSFCAG00000010080	ENSFCAG00000001933	ENSFCAG00000030943	ENSFCAG00000038719	ENSFCAG00000005681	ENSFCAG00000004982
Dog	ENSCAFG00000013283	ENSCAFG00000008499	ENSCAFG00000001710*	ENSCAFG00000012893	ENSCAFG00000001745*	ENSCAFG00000005444	ENSCAFG00000010220*	-	ENSCAFG00000015915	ENSCAFG00000024527	ENSCAFG00000016315	ENSCAFG00000017172	ENSCAFG00000005460	ENSCAFG00000023904	ENSCAFG00000011283	ENSCAFG00000015838	ENSCAFG00000024807*	ENSCAFG00000013576
Cow	ENSBTAG00000018253	ENSBTAG00000002252	ENSBTAG00000003130	ENSBTAG00000017198	ENSBTAG00000013657*	ENSBTAG00000014056	ENSBTAG00000015775	-	ENSBTAG00000015252	ENSBTAG00000055237	ENSBTAG00000019242	ENSBTAG00000007517	ENSBTAG00000014050	ENSBTAG00000003132	ENSBTAG00000011390*	ENSBTAG00000004908	ENSBTAG00000045943	ENSBTAG00000031330
Human	ENSG00000138435	ENSG00000120903	ENSG00000080644	ENSG00000101204	ENSG00000169684	ENSG00000147434	ENSG00000175344	-	ENSG00000074343	ENSG00000129749	ENSG00000170175	ENSG00000160716	ENSG00000147432	ENSG00000117971	ENSG00000135905	ENSG00000108556	ENSG00000196811	ENSG00000149305
Chimp	ENSPTRG00000012658	ENSPTRG00000020105	ENSPTRG00000007347	ENSPTRG00000013735	ENSPTRG00000007346	ENSPTRG00000020210	ENSPTRG00000006865	-	ENSPTRG00000016003	ENSPTRG00000003199	ENSPTRG00000008689	ENSPTRG00000001389	ENSPTRG00000020209	ENSPTRG00000007348	ENSPTRG00000013040	ENSPTRG00000008612	ENSPTRG00000022726	
Megabat	ENSPVAG00000004164	ENSPVAG00000014424	ENSPVAG00000009191	ENSPVAG00000014109	ENSPVAG00000009186	ENSPVAG00000015371*	ENSPVAG00000017796*	-	ENSPVAG00000003814	ENSPVAG00000016436	ENSPVAG00000005067	XM_023534307.1*	ENSPVAG00000015373	ENSPVAG00000009193	ENSPVAG00000007491	ENSPVAG00000000127	ENSPVAG00000007492*	
Microbat	ENSMLUG00000015698	ENSMLUG00000001512	-	Manual search on traces	-	ENSMLUG00000005231	ENSMLUG00000005856	-	ENSMLUG00000000893	ENSMLUG00000013586	ENSMLUG00000009921	ENSMLUG00000007541	ENSMLUG00000027322	-	ENSMLUG00000011213	ENSMLUG00000015682*	ENSMLUG00000011237	
Chick	ENSGALG00000009301	ENSGALG00000016565	ENSGALG00000003014	ENSGALG00000005801	ENSGALG00000003021	ENSGALG00000015382	ENSGALG00000004096	ENSGALG00000015336	ENSGALG00000014268	NM_001101036.1	-	ENSGALG00000002707	ENSGALG00000015384	ENSGALG00000003005	ENSGALG00000007899	-	ENSGALG00000007906	
Turkey	ENSMGAG00000009752	ENSMGAG00000014105	ENSMGAG00000003578	ENSMGAG00000006295	ENSMGAG00000003610*	-	ENSMGAG00000005132	-	ENSMGAG00000012228	XM_010706263.2	-	ENSMGAG00000006636*	ENSMGAG00000007510	ENSMGAG00000003559*	ENSMGAG00000008354	-	ENSMGAG00000008414	
Duck	ENSAPLG00000007803*	ENSAPLG00000009491*	ENSAPLG00000016121	ENSAPLG00000007776	ENSAPLG00000016223*	ENSAPLG00000012469	ENSAPLG00000010434	ENSAPLG00000007724	ENSAPLG00000013711*	-	-	ENSAPLG00000009547*	ENSAPLG00000012846	ENSAPLG00000016042	-	-	ENSAPLG00000015469*	
Flycatcher	ENSFALG00000003034	ENSFALG00000003731	ENSFALG00000010658	ENSFALG00000010418	ENSFALG00000010653	ENSFALG00000005209	ENSFALG00000012362*	ENSFALG00000001025	ENSFALG00000002853*	XM_016305564.1	-	ENSFALG00000001220	ENSFALG00000005194	ENSFALG00000010665	ENSFALG00000007740	-	ENSFALG00000007743	
Zebra finch	ENSTGUG00000008827	-	ENSTGUG00000003469	ENSTGUG00000007453	ENSTGUG00000003451*	ENSTGUG00000000216*	ENSTGUG00000005850	ENSTGUG00000000135	ENSTGUG00000008712	-	-	ENSTGUG00000004092	ENSTGUG00000000227	XM_002191803.3	-	-	ENSTGUG00000009924	
Anole lizard	ENSACAG00000005293	ENSACAG00000002388	-	ENSACAG00000005817	-	ENSACAG00000005512	ENSACAG00000008436	ENSACAG00000005448	ENSACAG00000011789	NW_003340045.1	-	ENSACAG00000015594	ENSACAG00000005630	-	ENSACAG00000010984	ENSACAG00000014790*	ENSACAG00000010910	
American alligator	XM_006267516.3	XM_006274660.2	XM_006261354.3	XM_019484414.1	XM_006261353.3	XM_006276967.2	XM_014599894.2	-	XM_019478038.1	XM_019480144.1	XM_006275274.2	XM_019497730	XM_006276963.2	XM_014605947	XM_019484776.1	-	NW_017709597.1*	
Chinese softshell turtle	ENSPSIG00000003348	ENSPSIG00000012597	ENSPSIG00000016882	ENSPSIG00000012045	-	ENSPSIG00000006517	ENSPSIG00000010525	ENSPSIG00000009608	ENSPSIG00000017539	XM_014580618.2	ENSPSIG00000009407	ENSPSIG00000006807*	ENSPSIG00000017586*	ENSPSIG00000017214	-	ENSPSIG00000003627*	ENSPSIG00000011304*	
Painted turtle	ENSCPBG00000003798	ENSCPBG00000022315	ENSCPBG00000024258	ENSCPBG00000027193	ENSCPBG00000024257	ENSCPBG00000027581*	-	-	ENSPSIG00000017539*	XM_024109380.1	ENSCPBG00000004679	ENSCPBG00000024641*	ENSCPBG00000027579	ENSCPBG00000024259	ENSCPBG00000016193	ENSCPBG00000016561*	ENSCPBG00000016190	
Xenopus tropicalis	ENSXETG00000025420	ENSXETG00000017553	ENSXETG00000031723	ENSXETG00000023746	ENSXETG00000023896*	ENSXETG00000010249*	ENSXETG00000016395	ENSXETG00000018003	ENSXETG00000012803	XM_002942872.4	-	ENSXETG00000003846	ENSXETG00000010250	ENSXETG00000033968*	ENSXETG00000027884	ENSXETG00000014957	ENSXETG00000013994*	ENSXETG00000031022
Tibetan frog	XM_018572442.1	XM_018570301.1	-	XM_018560101.1	-	XM_018557911.1	XM_018564234.1	-	XM_018564438.1	-	XM_018573841.1	XM_018570082.1	XM_018557907.1	XM_018572684.1	XM_018563344.1	-	XM_018572139.1	
Coelacanth	ENSLACG00000000109*	ENSLACG00000003345	XM_006001841.1	ENSLACG00000010383*	ENSLACG00000002798	-	ENSLACG00000005760*	-	ENSLACG00000009570	ENSLACG00000005922	ENSLACG00000008409	ENSLACG00000015217	ENSLACG00000002288	ENSLACG00000004838*	ENSLACG00000015676	ENSLACG00000002691	ENSLACG00000015771	
Fugu	XM_003961904.2	ENSTRUG00000008002*	ENSTRUG00000004067*	ENSTRUG00000010213	ENSTRUG00000005757	ENSTRUT00000002729.2	ENSTRUG00000016472	ENSTRUG00000002223	ENSTRUG00000010253	ENSTRUG00000003807	XM_011618734.1	ENSTRUG00000005762	ENSTRUG00000006363	ENSTRUG00000025609	ENSTRUG00000007767*	ENSTRUG00000016224	ENSTRUG00000014376*	ENSTRUG00000013084
						ENSTRUT00000016710.2	NC_018902.1	ENSTRUG00000005961	ENSTRUG00000013071	NW_004072435.1			ENSTRUG00000001764					
							NC_018896.1											
Medaka	XM_020713072.2	XM_011491375.3	ENSORLG00000013118	ENSORLG00000000865*	ENSORLG00000020077	ENSORLT00015028636.1	ENSORLG00000018774	ENSORLG00000003203	ENSORLG00000004390	NC_019871.2	-	ENSORLG00000009700	ENSORLG00000003226	ENSORLG00000013114	ENSORLG00000026994	ENSORLG00000008035*	-	ENSORLG00000014619
							ENSORLG00000030549	ENSORLG00000014282	ENSORLG00000005701	XM_011483838.3			ENSORLG00000014290					
Zebrafish	ENSDARG00000009021	NM_001040327.1	ENSDARG00000100991	NM_001048063.1	ENSDARG00000003420	ENSDARG00000055559	ENSDARG00000101522	ENSDARG00000087224	ENSDARG00000054680	NM_001044804.1	NM_001253810.1	ENSDARG00000017790	ENSDARG00000052764	ENSDARG00000101677	ENSDARG00000019342	ENSDARG00000034307	ENSDARG00000086647*	ENSDARG00000061749
							ENSDARG00000101702		ENSDARG00000099181	XM_021481417.1			ENSDARG00000038508					

Accession numbers correspond to Ensembl or Genbank databases. * Sequences mended and/or completed using trace fragments obtained from the NCBI Genome Project traces database.

Table S2. Mean percentage sequence identity (%seqID).

	All	Mammals	Mammals-Sauropsid	Sauropsid
CHRNA1	83.98 (26)	93.40 (11)	85.44	88.98 (9)
CHRNA2	73.99 (24)	81.02 (11)	71.68	82.21 (7)
CHRNA3	80.91 (23)	89.78 (10)	83.50	91.79 (8)
CHRNA4	73.63 (26)	80.77 (11)	74.14	90.06 (9)
CHRNA5	84.55 (21)	90.65 (9)	86.18	96.27 (7)
CHRNA6	77.61 (24)	88.09 (11)	80.31	84.93 (8)
CHRNA7	79.22 (26)	92.97 (9)	89.69	96.97 (8)
CHRNA8	77.63 (12)	-	-	91.49 (6)
CHRNA9	72.16 (29)	90.90 (11)	74.23	88.28 (9)
CHRNA10	64.93 (24)	88.98 (11)	61.29	75.38 (5)
CHRNB1	70.47 (18)	86.24 (11)	63.82	73.20 (3)
CHRNB2	77.16 (26)	88.70 (11)	75.83	76.87 (9)
CHRNB3	81.47 (28)	88.41 (11)	84.59	91.83 (8)
CHRNB4	72.12 (23)	80.83 (10)	71.75	85.65 (7)
CHRND	71.54 (22)	87.85 (10)	68.02	76.59 (6)
CHRNE	67.34 (16)	83.08 (10)	58.60	-
CHRNG	69.12 (24)	86.81 (11)	63.41	79.55 (8)

Values were calculated using pairs of sequences of all vertebrates, mammals or sauropsids nAChRs subunits. (n) Indicates the number of orthologues from each subunit included in the calculations. White background: muscle subunits; light background grey: neuronal subunits; dark grey background: hair cells subunits.

Table S3. Type II functional divergence coefficients for nAChR subunits

	θ_{II} ± SE	P value	N sites
CHRNA1	0.0082 ± 0.03	0.41	1
CHRNA2	-0.02 ± 0.03	0.23	0
CHRNA3	0.03 ± 0.03	0.19	1
CHRNA4	0.01 ± 0.03	0.33	0
CHRNA5	0.03 ± 0.03	0.12	2
CHRNA6	0.01 ± 0.03	0.41	0
CHRNA7	0.02 ± 0.02	0.16	3
CHRNA9	0.05 ± 0.02	0.038	15
CHRNA10	0.1 ± 0.04	0.0071	10
CHRNB2	0.01 ± 0.02	0.30	0
CHRNB3	0.02 ± 0.03	0.29	1
CHRNB4	0.05 ± 0.03	0.060	1
CHRND	0.03 ± 0.05	0.28	4
CHRNG	0.08 ± 0.05	0.051	3

θ_{II}, coefficient of type II functional divergence. SE, standard error. N sites, number of residues per nicotinic subunit with posterior probabilities for type II functional divergence greater than 0.65.

Table S4. Single-cell RNA sequencing datasets.

Publication	DOI	Accession	Tissue	mean_genes	Cell_types	#Cells
Shekar, et al. 2016	10.1016/j.cell.2016.07.054	GSE81905	Retina	5372	BC1A	14
					BC5A	24
					BC6	17
					RBC	99
Chevee, et al. 2018	10.1016/j.celrep.2017.12.046	GSE107632	Somatosensory cortex	5614	VPMonly	130
					VPM/Pom	210
Cembrowski, et al. 2018	10.1016/j.cell.2018.03.031	GSE100449	Hippocampus	5218	dSub	72
					pSub1	69
					pSub2	102
Romanov	10.1038/nn.4462	GSE74672	Hypothalamus	3887	Adcyap1	34
					Avp	25
					Dopamine	41
					GABA	311
					circadian	31
					Hmit	24
					Oxytocin	37
					Sst	38
					Trh	55
					Vglut2	137
LaManno, et al. 2016	10.1016/j.cell.2016.09.027	GSE76381	Ventral midbrain	4106	DA_SNC	73
					DA_VTA1	47
					DA_VTA2	28
					DA_VTA3	26
					DA_VTA4	69
Shrestha, et al. 2018	10.1016/j.cell.2018.07.007	GSE114997	Spiral ganglion	8298	SGN_TypeIa	63
					SGN_TypeIb	71
					SGN_TypeIc	45
McInturff	10.1242/bio.038083	GSE115934.	utricle HC	5578	HC_P1	37
					HC_P12	50
					HC_P100	25
Burns	10.1038/ncomms9557	GSE71982	inner ear	7143	Co_HC	10
Furlan, et al. 2016	10.1038/nn.4376	GSE78845	Sympathetic ganglion	6297	Nor1	10
					Nor2	39
					Nor3	103
					Nor4	18
					Nor5	23
					Glu	4
					Ach1	8
					Ach2	8
Usoskin	10.1038/nn.3881	GSE59739	DRG	3821	NF1	21
					NF2	43
					NF3	10
					NF4	16
					NF5	24
					NP1	80
					NP2	19
					NP3	10
					PEP1	50
					PEP2	14
					TH	142

Accession information for the datasets used on the analysis of nAChR subunits co-expression patterns. mean_genes, average number of genes per cell detected in each dataset. Cell_types, final cell types, as inferred in each publication, used to estimate the expression levels of nAChR subunit genes. #Cells, number of cells for each cell type present in the final datasets analysed.

Table S5. Mean expression of nAChR subunits genes across cell types.

	Retina				Somatosensory cortex		Hippocampus			Hypothalamus									
	BC1A	BC5A	BC6	RBC	VPM-only	VPM/Pom	dSub	pSub1	pSub2	Adcyap1	Avp	Dopamine	GABA	circadian	Hmit	Oxytocin	Sst	Trh	Vglut2
Chrna1	3.46	0.72	3.18	1.24	0.00	0.00	0.00	0.00	0.00	0.00	0.00	0.00	0.00	0.00	24.85	0.00	0.00	0.00	0.00
Chrna2	2.93	1.41	3.17	1.37	0.00	0.00	0.00	0.00	0.00	0.00	0.00	0.00	0.00	0.00	0.00	0.00	0.00	0.00	0.00
Chrna3	0.00	0.00	0.00	13.35	0.00	0.00	0.00	0.00	0.00	8.33	0.00	62.03	5.92	0.00	59.68	0.00	8.54	0.00	9.97
Chrna4	382.03	52.93	25.66	6.74	92.58	100.99	99.88	6.10	30.51	68.76	14.87	80.34	43.55	10.23	37.64	17.36	0.00	17.47	100.82
Chrna5	5.35	2.48	3.18	8.01	3.05	13.80	5.36	0.00	2.68	0.00	0.00	0.00	4.89	0.00	0.00	0.00	0.00	0.00	0.00
Chrna6	267.64	0.00	601.04	10.78	0.00	0.00	0.00	0.00	0.00	0.00	0.00	5.67	0.00	0.00	0.00	0.00	0.00	0.00	0.00
Chrna7	19.29	52.13	0.00	0.00	20.54	11.37	0.00	0.00	0.00	5.39	0.00	0.00	7.56	0.00	0.00	0.00	0.00	0.00	0.00
Chrna9	0.00	0.00	0.00	0.00	0.00	0.00	0.00	0.00	0.00	0.00	0.00	0.00	0.00	0.00	0.00	0.00	0.00	0.00	0.00
Chrna10	0.88	0.00	0.00	0.00	0.00	0.00	0.00	0.00	0.00	0.00	0.00	0.00	4.53	0.00	0.00	0.00	0.00	0.00	0.00
Chrnb1	34.77	55.02	28.26	17.92	0.00	0.00	0.00	0.00	0.00	0.00	8.59	0.00	3.98	0.00	0.00	0.00	0.00	0.00	0.00
Chrnb2	78.90	23.43	134.51	25.77	43.13	31.83	15.83	13.12	24.99	83.16	21.37	99.08	55.77	35.06	53.54	75.05	92.14	50.69	79.18
Chrnb3	43.53	0.46	138.25	5.91	0.00	0.00	0.00	0.00	0.00	0.00	0.00	0.00	4.86	0.00	0.00	0.00	0.00	0.00	0.00
Chrnb4	4.68	1.14	2.02	1.33	0.00	0.00	0.00	0.00	0.00	0.00	0.00	0.00	0.00	0.00	0.00	0.00	0.00	0.00	0.00
Chrnd	0.00	0.00	0.00	0.00	0.00	0.00	0.00	0.00	0.00	0.00	0.00	0.00	0.00	0.00	0.00	0.00	0.00	0.00	0.00
Chrne	0.00	0.00	0.00	0.00	0.00	0.00	0.00	0.00	0.00	0.00	0.00	0.00	0.00	0.00	0.00	0.00	0.00	0.00	0.00
Chrng	0.00	0.00	0.00	0.00	0.00	0.00	0.00	0.00	0.00	0.00	0.00	0.00	0.00	0.00	0.00	0.00	0.00	0.00	0.00

	Ventral midbrain					Spiral ganglion			Inner ear hair cells			
	SNC	VTA1	VTA2	VTA3	VTA4	TypeIa	TypeIb	TypeIc	Utricle_HC_P1	Utricle_HC_P12	Utricle_HC_P100	Cochlear_HC
Chrna1	0.00	0.00	0.00	0.00	0.00	76.33	5.52	27.55	320.99	376.92	388.80	154.91
Chrna2	0.00	0.00	0.00	0.00	0.00	0.00	0.00	0.00	0.00	0.00	0.00	0.00
Chrna3	75.04	61.02	34.75	0.00	9.22	0.00	0.00	16.67	0.00	0.00	0.00	0.00
Chrna4	559.44	674.74	277.56	568.53	274.87	131.75	57.37	18.66	0.00	0.00	0.00	0.00
Chrna5	28.65	16.99	19.36	0.00	3.32	0.00	0.00	0.00	0.00	0.00	0.00	0.00
Chrna6	1286.75	718.59	1140.92	705.52	821.02	0.00	0.00	11.64	0.00	0.00	0.00	0.00
Chrna7	0.00	0.00	0.00	0.00	0.00	37.61	49.86	21.04	0.00	0.00	0.00	0.00
Chrna9	0.00	0.00	0.00	0.00	0.00	15.33	13.61	0.00	554.41	626.98	607.56	350.02
Chrna10	0.00	0.00	0.00	0.00	0.00	0.00	4.42	7.33	464.02	632.15	599.18	466.89
Chrnb1	0.00	0.00	0.00	0.00	0.00	80.87	59.75	76.27	15.00	39.59	26.26	39.70
Chrnb2	37.12	100.00	91.58	117.53	70.01	298.16	295.47	315.08	96.02	175.77	182.60	62.75
Chrnb3	326.52	370.87	260.30	351.18	344.16	0.00	3.64	11.32	0.00	0.00	0.00	0.00
Chrnb4	0.00	0.00	0.00	0.00	0.00	4.39	18.07	0.00	24.11	22.30	2.31	4.21
Chrnd	0.00	0.00	0.00	0.00	0.00	0.00	0.00	0.00	0.00	0.00	0.00	2.35
Chrne	0.00	0.00	0.00	0.00	0.00	4.97	5.00	7.81	0.00	5.92	22.78	0.00
Chrng	0.00	0.00	0.00	0.00	0.00	0.00	0.00	0.00	509.75	40.42	0.00	32.97

	Visceral motor neurons								Dorsal root ganglia										
	Nor1	Nor2	Nor3	Nor4	Nor5	Glut	Ach1	Ach2	NF1	NF2	NF3	NF4	NF5	NP1	NP2	NP3	PEP1	PEP2	TH
Chrna1	0.00	0.00	0.00	0.00	0.00	0.00	0.00	0.00	0.00	0.00	15.18	0.00	0.00	0.00	0.00	0.00	0.00	0.00	0.79
Chrna2	0.00	0.00	0.00	0.00	0.00	0.00	0.00	0.00	0.00	0.00	0.00	0.00	0.00	0.00	0.00	0.00	0.00	0.00	0.00
Chrna3	535.34	689.45	825.02	808.62	988.48	107.72	572.22	596.98	0.00	0.00	0.00	0.00	0.00	0.00	0.00	0.00	0.00	40.86	0.00
Chrna4	0.00	0.00	0.00	0.00	0.00	0.00	9.93	0.00	0.00	3.45	0.00	0.00	0.00	0.00	0.00	44.71	0.00	0.00	28.78
Chrna5	55.99	50.79	41.92	38.86	38.83	0.00	51.51	37.33	0.00	0.00	0.00	0.00	0.00	0.00	0.00	0.00	0.00	0.00	0.00
Chrna6	0.00	0.00	0.00	0.00	0.00	79.15	0.00	0.00	76.83	4.69	0.00	0.00	0.00	95.66	128.57	126.53	89.34	0.00	6.40
Chrna7	12.13	30.63	39.57	15.58	9.06	0.00	0.00	8.86	0.00	0.00	9.14	0.00	0.00	0.00	0.00	0.00	0.00	15.08	0.00
Chrna9	0.00	0.00	0.00	0.00	0.00	0.00	0.00	0.00	0.00	0.00	0.00	0.00	0.00	0.00	0.00	0.00	0.00	0.00	0.00
Chrna10	0.00	0.00	0.00	0.00	0.00	0.00	0.00	0.00	0.00	0.00	3.03	0.00	0.00	0.00	0.00	0.00	0.00	17.27	0.00
Chrnb1	0.00	0.00	0.00	0.00	0.00	0.00	7.76	0.00	0.00	0.00	0.00	0.00	0.00	0.00	0.00	0.00	11.97	0.00	0.00
Chrnb2	90.59	50.45	60.37	46.26	56.20	42.76	62.82	61.41	62.69	45.23	134.24	25.43	61.54	79.49	21.35	59.17	25.69	50.66	47.42
Chrnb3	0.00	0.00	0.00	0.00	0.00	109.59	0.00	0.00	0.00	0.00	0.00	0.00	0.00	4.15	0.00	0.00	9.39	0.00	1.70
Chrnb4	154.87	202.31	264.13	290.53	232.07	42.76	222.23	164.63	0.00	0.00	0.00	0.00	0.00	1.81	0.00	0.00	0.00	23.00	0.00
Chrnd	0.00	0.00	0.00	0.00	0.00	0.00	0.00	0.00	0.00	0.00	0.00	0.00	0.00	0.00	8.76	0.00	0.00	0.00	0.00
Chrne	0.00	0.00	0.00	0.00	0.00	0.00	0.00	0.00	0.00	0.00	0.00	0.00	0.00	0.00	0.00	0.00	0.00	0.00	0.00
Chrng	0.00	0.00	0.00	0.00	0.00	0.00	0.00	0.00	0.00	0.00	0.00	0.00	0.00	0.00	0.00	0.00	0.00	0.00	0.00

Values are means of the estimated joint posterior distributions of gene expression levels inferred for the nAChR subunits expressed in the cell types and datasets analysed.

Table S6. Neuronal nAChRs experimentally validated assemblies.

nAChR subtype	DOI	Reference
α7	10.1016/0896-6273(90)90344-F	Couturier et al., 1990
α8	PMID: 7509438	Gerzanich et al., 1994
α9	10.1016/0092-8674(94)90555-X	Elgoyhen 1994 et al., 1994
α10	10.1093/molbev/msu258	Lipovsek et al., 2014
α2β2	10.1016/0896-6273(88)90208-5	Deneris et al., 1988
α2β4	10.1016/0896-6273(89)90207-9	Duvoisin et al.,1989
α3β2	10.1073/pnas.84.21.7763	Boulter et al., 1987
α3β4	10.1016/0896-6273(89)90207-9	Duvoisin et al.,1989
α4β2	10.1073/pnas.84.21.7763	Boulter et al., 1987
α4β4	10.1016/0896-6273(89)90207-9	Duvoisin et al., 1989
α6β2	10.1046/j.1460-9568.1998.00001.x	Fucile et al., 1998
α6β4	10.1124/mol.106.027326	Tumkosit et al., 2006
α7β2	10.1113/jphysiol.2001.013847	Khiroug et al., 2002
α7β3	10.1074/jbc.274.26.18335	Palma etal., 1999
α7β4	110.1111/j.1471-4159.2012.07931.x	Criado et al., 2012
α9α10	10.1073/pnas.051622798	Elgoyhen et al., 2001
α2α5β2	10.1124/mol.63.6.1329	Vailati et al., 2003
α2α6β2	10.1124/mol.105.015925	Gotti et al., 2005
α2β2β3	10.1111/j.1471-4159.2012.07685.x	Dash et al., 2012
α2β3β4	10.1111/j.1471-4159.2012.07685.x	Dash et al., 2012
α3α4β2	10.1523/JNEUROSCI.2112-05.2005	Turner et al., 2005
α3α4β4	10.1523/JNEUROSCI.2112-05.2005	Turner et al., 2005
α3α5β2	10.1074/jbc.271.30.17656	Wang et al., 1996
α3α5β4	10.1074/jbc.271.30.17656	Wang et al., 1996
α3α6β2	10.1016/S0028-3908(00)00144-1	Kuryatov et al., 2000
α3α6β4	10.1046/j.1460-9568.1998.00001.x	Fucile et al., 1998
α3β2β4	10.1523/JNEUROSCI.2112-05.2005	Turner et al., 2005
α3β2β3	10.1111/j.1471-4159.2012.07685.x	Dash et al., 2012
α3β3β4	10.1074/jbc.273.25.15317	Groot-Kormelink et al., 1998
α4α5β2	10.1038/380347a0	Ramirez-Latorre et al., 1996
α4β2β3	10.1124/mol.108.046789	Kuryatov et al., 2008
α4β3β4	10.1111/j.1471-4159.2012.07685.x	Dash et al., 2012
α5α6β2	10.1016/S0028-3908(00)00144-1	Kuryatov et al., 2000
α5α7β2	10.1111/j.1749-6632.1999.tb11331.x	Girod et al., 1999
α6β2β3	10.1124/mol.106.027326	Tumkosit et al., 2006
α6β3β4	10.1016/S0028-3908(00)00144-1	Kuryatov et al., 2000
α3α4α6β2	10.1111/j.1471-4159.2008.05282.x	Cox etal., 2008
α3α5β2β4	10.1074/jbc.270.9.4424	Conroy and Berg, 1995
α4α6β2β3	10.1124/mol.110.066159	Kuryatov and Lindstrom, 2010
α5α6β3β4	10.1124/jpet104.075069	Grinevich et al., 2005
α1β1γδ	10.1038/321406a0	Mishina et al., 1986
α1β1δε	10.1038/321406a0	Mishina et al., 1986

Experimentally validated pentameric combinations of nAChR subunits and relevant literature references.

Table S7. Primers used for the cloning of *X. tropicalis* nAChRs subunits.

Primer	Tm (ºC)	Sequence (5'-3')
FXtrop.a9	61.4	TA**GAATTC**ATGCACACATTTTTGGCACGTGTTGG
RXtrop.a9	63.1	AT**CTCGAG**TCACACTGCCTGGGCAATAA
FXtrop.a10	62.4	AT**AAGCTT**TCCTGCCCAACATGAGACTGC
RXtrop.a10	62.1	AT**CTCGAG**GGCACCATCATATGGCTTTG
FXtrop.a7	61.8	TA**GAATTC**TTTGATCTCCTGCGATGGGAGGA
RXtrop.a7	61.9	AT**CTCGAG**TAGAACTGCAGAACCCTAAGCAA
FXtrop.a4	62.7	AT**GAATTC**GCTCTCTGCCAACATGGGTG
RXtrop.a4	60.1	TA**AAGCTT**GGGGTCAGTTCATATCAAACCAG
FXtrop.b2	61.2	TA**GAATTC**GAGGCGATGAGATGATCCGG
RXtrop.b2	61.3	AT**CTCGAG**GCCCTCAATGTTTCTCAGTT

The restriction sites for EcoRI, XhoI and HindIII used for subsequent subcloning are highlighted in bold. Tm, annealing temperature.

Table S8. Biophysical properties and statistical comparisons from rat, chicken and frog α4β2, α7 and α9α10 receptors.

Receptor		**α4β2**					
Species		Rat		Chicken		Frog	
ACh sensitivity	Mean ± S.E.M (n)	3.11 ± 2.11 (3)	159.76 ± 35.67 (4)	1.07 ± 0.15 (6)	66.00 ± 9.76 (4)	0.75 ± 0.02 (7)	143.71 ± 51.89 (5)
	ANOVA (p-value)	EC50_1: Rat vs Chick = 0.1346, Rat vs Frog = 0.1018, Chick vs Frog = 0.6927^{P}					
		EC50_2: Rat vs Chick = 0.3743, Rat vs Frog = 0.7809, Chick vs Frog = 0.3743^{P}					
Desensitization	Mean ± S.E.M (n)	77.13 ± 1.21 (4)		77.68 ± 5.16 (7)		72.70 ± 3.04 (10)	
	ANOVA (p-value)	Rat vs Chick = 0.9336, Rat vs Frog = 0.7326, Chick vs Frog = 0.7204^{P}					
Ca^{2+} Modulation	Mean ± S.E.M (n)	0.36 ± 0.04 (5)		0.55 ± 0.03 (9)		0.60 ± 0.08 (5)	
	ANOVA (p-value)	Rat vs Chick > 0.999, Rat vs Frog > 0.9999, Chick vs Frog > 0.9999^{P}					
Ca^{2+} Permeability	Mean ± S.E.M (n)	72.07 ± 9.62 (4)		78.75 ± 5.04 (6)		81.51 ± 7.91 (6)	
	ANOVA (p-value)	Rat vs Chick = 0.7999, Rat vs Frog = 0.7892, Chick vs Frog = 0.7999^{P}					
Rectification profile	Mean ± S.E.M (n)	0.07 ± 0.03 (5)		0.03 ± 0.03 (6)		0.02 ± 0.03 (6)	
	ANOVA (p-value)	Rat vs Chick = 0.6838, Rat vs Frog = 0.4995, Chick vs Frog = 0.9437^{P}					
Receptor		**α7**					
Species		Rat		Chicken		Frog	
ACh sensitivity	Mean ± S.E.M (n)	432.1 ± 123.45 (8)		267.56 ± 87.98 (8)		239.27 ± 33.90 (7)	
	ANOVA (p-value)	Rat vs Chick = 0.365, Rat vs Frog = 0.6723, Chick vs Frog > 0.9999^{NP}					
Desensitization	Mean ± S.E.M (n)	3.23 ± 0.79 (6)		3.18 ± 0.54 (9)		2.00 ± 0.41 (6)	
	ANOVA (p-value)	Rat vs Chick > 0.9999, Rat vs Frog = 0.3743, Chick vs Frog = 0.2496^{NP}					
Ca^{2+} Modulation	Mean ± S.E.M (n)	0.63 ± 0.10 (4)		0.46 ± 0.06 (4)		0.63 ± 0.08 (4)	
	ANOVA (p-value)	Rat vs Chick > 0.999, Rat vs Frog > 0.9999, Chick vs Frog > 0.9999^{P}					
Ca^{2+} Permeability	Mean ± S.E.M (n)	29.07 ± 7.68 (4)		37.10 ± 11.82 (4)		38.47 ± 3.98 (7)	
	ANOVA (p-value)	Rat vs Chick = 0.7447, Rat vs Frog = 0.7447, Chick vs Frog = 0.8931^{P}					
Rectification profile	Mean ± S.E.M (n)	0.04 ± 0.02 (5)		0.02 ± 0.003 (5)		0.03 ± 0.01 (5)	
	ANOVA (p-value)	Rat vs Chick = 0.5909, Rat vs Frog = 0.9706, Chick vs Frog = 0.7295^{P}					
Receptor		**α9α10**					
Species		Rat		Chicken		Frog	
ACh sensitivity	Mean ± S.E.M (n)	19.39 ± 2.08 (9)		17.62 ± 3.33 (6)		110.89 ± 25.00 (7)	
	ANOVA (p-value)	Rat vs Chick > 0.9999, Rat vs Frog = 0.0026**, Chick vs Frog = 0.006**^{NP}					
Desensitization	Mean ± S.E.M (n)	64.46 ± 3.65 (5)		60.84 ± 4.23 (9		14.53 ± 3.01 (7)	
	ANOVA (p-value)	Rat vs Chick > 0.9999, Rat vs Frog = 0.0051**, Chick vs Frog = 0.0042**^{NP}					
Ca^{2+} Modulation	Mean ± S.E.M (n)	3.76 ± 0.73 (5)		1.00 ± 0.07 (4)		0.63 ± 0.05 (12)	
	ANOVA (p-value)	Rat vs Chick < 0.0001****, Rat vs Frog < 0.0001****, Chick vs Frog > 0.9981^{P}					
Ca^{2+} Permeability	Mean ± S.E.M (n)	24.89 ± 2.81 (6)		100.28 ± 14.02 (6)		19.56 ± 3.38 (10)	
	ANOVA (p-value)	Rat vs Chick = 0.0299*, Rat vs Frog > 0.9999, Chick vs Frog = 0.0013**^{NP}					
Rectification profile	Mean ± S.E.M (n)	1.21 ± 0.07 (11)		2.31 ± 0.34 (10)		0.21 ± 0.05 (8)	
	ANOVA (p-value)	Rat vs Chick = 0.0229*, Rat vs Frog = 0.0406*, Chick vs Frog < 0.0001****^{NP}					

Values are shown as mean ± S.E.M. (n). ^{P}: parametric, ^{NP}: non-parametric analysis. ACh sensitivity: EC_{50} value; Desensitization rate: percentage current remaining 20 seconds (5 sec for α7 receptors) after peak response to a 10-fold concentration of EC_{50} ACh; Ca^{2+} Modulation: current elicited by EC_{50} ACh at Ca^{2+} 0.5 mM relative to Ca^{2+} 3 mM; Ca^{2+} Permeability: percentage of remaining current after BAPTA-AM treatment; Rectification profile: current recorded at +40 mV relative to that recorded at -90 mV.

Table S9. Normalized biophysical properties

Receptor	ACh sensitivity (EC_{50})	Desensitization (%*I* after ACh peak)	Ca^{2+} modulation ($I_{0.5\ mM}/I_{3\ mM}$)	Ca^{2+} permeability (%*I* post-BAPTA)	Rectification ($I_{+40\ mV}/I_{-90\ mV}$)
Rat α9α10	0.045	0.830	1.000	0.248	0.525
Chick α9α10	0.041	0.783	0.266	1.000	1.000
Frog α9α10	0.257	0.187	0.167	0.195	0.091
Rat α4β2	0.007	0.993	0.097	0.719	0.029
Chick α4β2	0.002	1.000	0.146	0.785	0.014
Frog α4β2	0.002	0.936	0.158	0.813	0.008
Rat α7	1.000	0.042	0.167	0.290	0.016
Chick α7	0.619	0.041	0.121	0.370	0.009
Frog α7	0.554	0.026	0.168	0.384	0.015
Amniote α4β2	0.004	0.985	0.128	0.762	0.019
Tetrapod α4β2	0.003	0.963	0.141	0.785	0.014
Amniote α7	0.679	0.038	0.141	0.357	0.012
Tetrapod α7	0.675	0.037	0.142	0.358	0.012
Amniote α9α10	0.114	0.594	0.409	0.549	0.581
Tetrapod α9α10	0.139	0.522	0.366	0.487	0.494

Normalized biophysical properties from extant receptors used in PCA analysis (top) and normalised inferred biophysical properties from ancestral receptors. Values are normalised relative to the maximum obtained for each parameter.

Table S10. PCA analysis of functional properties.

	PC1	PC2	PC3	PC4	PC5
ACh sensitivity (EC_{50})	0.55	0.04	0.35	0.72	0.23
Desensitization (%*I* after ACh peak)	-0.56	-0.11	-0.35	0.41	0.62
Ca^{2+} modulation ($I_{0.5\ mM}/I_{3\ mM}$)	-0.18	0.77	-0.26	0.36	-0.42
Ca^{2+} permeability (%*I* post-BAPTA)	-0.46	-0.46	0.37	0.38	-0.55
Rectification ($I_{+40\ mV}/I_{-90\ mV}$)	-0.36	0.42	0.74	-0.21	0.31
Proportion of the variability	0.54	0.28	0.14	0.03	0.006
Accumulated proportion	0.54	0.82	0.96	0.99	1.00

Upper panel: loading of each experimental parameter on the five principal components. *Lowe panel*: proportion and accumulated proportion of the variability represented by each principal component.

Table S11. Estimated distances between extant and inferred ancestral α9α10, α4β2 and α7 nAChRs based on protein sequence identity.

α4β2		
Comparison	**seqID**	**1-seqID**
Rat-amniote	0.824	0.176
Chick-amniote	0.816	0.184
Amniote-tetrapod	0.819	0.181
Frog-tetrapod	0.777	0.223

α7		
Comparison	**seqID**	**1-seqID**
Rat-amniote	0.888	0.112
Chick-amniote	0.962	0.038
Amniote-tetrapod	0.997	0.003
Frog-tetrapod	0.907	0.093

α9α10		
Comparison	**seqID**	**1-seqID**
Rat-amniote	0.683	0.317
Chick-amniote	0.821	0.179
Amniote-tetrapod	0.96	0.04
Frog-tetrapod	0.814	0.186

Sequence identity (seqID) values between pairs of sequences were calculated using the protein sequence alignments in Supplementary File 3). Distances (1-seqID values) were subsequently used as branch lengths for the receptor trees used for the inference of ancestral character states for each nAChR (Fig. S6).

Supplementary File Legends

Supplementary File 1. Multiple alignment of nAChRs subunits. The alignment includes 392 nAChR subunits sequences from 29 different species together with 9 sequences from 5HT3B vertebrate subunits (outgroup).

Supplementary File 2. Aminoacid sequence identities. Values for all pairwise comparisons for all nAChR subunits from amniotes.

Supplementary File 3. Type II functional divergence analysis using DIVERGE 3.0. For each nAChR subunit analysed, the main tree, cluster-mammalian tree and cluster-sauropsid tree are shown in parenthetical notation. Theta-II values and standard error (SE) were calculated by comparing the designated clusters. Posterior probabilities (Pp) per site were calculated from the Posterior ratio (Pr) values obtained from the type II function by *Pp = Pr / (1+Pr)*, as in Gu et al, 2006.

Supplementary File 4. Sequences used for the reconstruction of ancestral nAChR subunits. DNA sequences from α4, α7, α9, α10 and β2 orthologues used to reconstruct DNA sequences from amniote and tetrapod ancestors. The species trees, in parenthetic format, are shown before the sequence alignment, in fasta format. The branch lengths in the species trees were inferred from each alignment and indicate the amount of accumulated changes.

Supplementary File 5. Extant and inferred ancestral nAChRs protein sequences. Protein sequences from rat, chicken, frog, amniote ancestor and tetrapod ancestor, from α7, $(\alpha4)_2(\beta2)_3$ and $(\alpha9)_2(\alpha10)_3$ nAChRs were aligned and the sequence identity between pairs of receptors was used to calculate the branch lengths assigned to the receptor trees (Supplementary Figure 6) used to infer ancestral character states of biophysical properties (Supplementary Figure 7).

Supplementary Information References

1. Kumar S, Stecher G, & Tamura K (2016) MEGA7: Molecular Evolutionary Genetics Analysis Version 7.0 for Bigger Datasets. *Mol Biol Evol* 33(7):1870-1874.
2. Jones DT, Taylor WR, & Thornton JM (1992) The rapid generation of mutation data matrices from protein sequences. *Comput Appl Biosci* 8(3):275-282.
3. Saitou N & Nei M (1987) The neighbor-joining method: A new method for reconstructing phylogenetic trees. *Mol Biol Evol* 4(4):406-425.
4. Felsenstein J (1985) Confidence limits on phylogenies: an approach using the bootstrap. *Evolution* 39(4):783-791.
5. Rzhetsky A & Nei M (1992) A simple method for estimating and testing minimum-evolution trees. *Mol Biol Evol* 9(5):945-967.
6. Gu X (2006) A simple statistical method for estimating type-II (cluster-specific) functional divergence of protein sequences. *Mol Biol Evol* 23(10):1937-1945.
7. Gu X*, et al.* (2013) An update of DIVERGE software for functional divergence analysis of protein family. *Mol Biol Evol* 30(7):1713-1719.
8. Shekhar K*, et al.* (2016) Comprehensive Classification of Retinal Bipolar Neurons by Single-Cell Transcriptomics. *Cell* 166(5):1308--1323.e1330.
9. Burns JC, Kelly MC, Hoa M, Morell RJ, & Kelley MW (2015) Single-cell RNA-Seq resolves cellular complexity in sensory organs from the neonatal inner ear. *Nature Communications* 6:1-16.
10. McInturff S, Burns JC, & Kelley MW (2018) Characterization of spatial and temporal development of Type I and Type II hair cells in the mouse utricle using new cell-type-specific markers. *Biology open* 7(11).
11. Shrestha BR*, et al.* (2018) Sensory neuron diversity in the inner ear is shaped by activity sensory neuron diversity. *Cell* 174:1229-1246.
12. La Manno G*, et al.* (2016) Molecular diversity of midbrain development in resource molecular diversity of midbrain development in mouse, human and stem cells. *Cell* 167:566-580.
13. Cembrowski MS*, et al.* (2018) Dissociable Structural and Functional Hippocampal Outputs via Distinct Subiculum Cell Classes. *Cell* 173(5):1280--1292.e1218.
14. Chevée M, Robertson JDJ, Cannon GH, Brown SP, & Goff LA (2018) Variation in Activity State, Axonal Projection, and Position Define the Transcriptional Identity of Individual Neocortical Projection Neurons. *Cell Reports* 22(2):441-455.
15. Romanov RA*, et al.* (2017) Molecular interrogation of hypothalamic organization reveals distinct dopamine neuronal subtypes. *Nature Neuroscience* 20(2):176-188.
16. Furlan A*, et al.* (2016) Visceral motor neuron diversity delineates a cellular basis for nipple- and pilo-erection muscle control. *Nature Neuroscience* 19(10):1331-1340.
17. Usoskin D*, et al.* (2015) Unbiased classification of sensory neuron types by large-scale single-cell RNA sequencing. *Nature Neuroscience* 18(1):145-153.
18. McCarthy DJ, Campbell KR, Lun AT, & Wills QF (2017) Scater: pre-processing, quality control, normalization and visualization of single-cell RNA-seq data in R. *Bioinformatics* 33(8):1179-1186.
19. Lun AT, Bach K, & Marioni JC (2016) Pooling across cells to normalize single-cell RNA sequencing data with many zero counts. *Genome biology* 17:75.
20. Kharchenko PV, Silberstein L, & Scadden DT (2014) Bayesian approach to single-cell differential expression analysis. *Nature Methods* 11(7):740-742.
21. Elgoyhen AB, Johnson DS, Boulter J, Vetter DE, & Heinemann S (1994) α9: an acetylcholine receptor with novel pharmacological properties expressed in rat cochlear hair cells. *Cell* 79(4):705-715.

22. Elgoyhen AB*, et al.* (2001) α10: a Determinant of Nicotinic Cholinergic Receptor Function in Mammalian Vestibular and Cochlear Mechanosensory Hair Cells. *Proc.Natl.Acad.Sci.U.S.A.* 98(6):3501-3506.
23. Lipovsek M*, et al.* (2012) Phylogenetic differences in calcium permeability of the auditory hair cell cholinergic nicotinic receptor. *Proc.Natl.Acad.Sci.U.S.A.* 109(11):4308-4313.
24. Gerzanich V, Anand R, & Lindstrom JM (1994) Homomers of α8 and α7 subunits of nicotinic receptors exhibit similar channel but contrasting binding site properties. *Molecular Pharmacology* 45(2):212 LP-- 220.
25. Weisstaub N, Vetter DE, Elgoyhen AB, & Katz E (2002) The α9α10 nicotinic acetylcholine receptor is permeable to and is modulated by divalent cations. *Hearing Research* 167(1-2):122-135.
26. Arellano RO, Woodward RM, & Miledi R (1995) A monovalent cationic conductance that is blocked by extracellular divalent cations in Xenopus oocytes. *J Physiol* 484 (Pt 3):593-604.
27. Ebihara L (1996) Xenopus connexin38 forms hemi-gap-junctional channels in the nonjunctional plasma membrane of Xenopus oocytes. *Biophysical journal* 71(2):742-748.
28. Nei M & Kumar S (2000) *Molecular Evolution and Phylogenetics* (Oxford Press, New York).
29. Tamura K & Nei M (1993) Estimation of the number of nucleotide substitutions in the control region of mitochondrial DNA in humans and chimpanzees. *Mol Biol Evol* 10(3):512-526.
30. Paradis E, Claude J, & Strimmer K (2004) APE: Analyses of phylogenetics and evolution in R language. *Bioinformatics* 20(2):289-290.
31. Schluter D, Price T, Mooers A, & Ludwig D (1997) Likelihood of Ancestors States in Adaptive Radiation. *Evolution* 51(6):1699-1711.
32. Felsenstein J (1973) Maximum-Likelihood Estimation of Evolutionary Trees from Continuous Characters. *Am J Hum Genet* 25:471-492.